

PR-01-005 Update to Jefferson Lab PAC 21

Measurement of the Weak Pion-Nucleon Coupling
Constant, h_{π}^1 , in Parity-Violating Backward Pion
Photoproduction near Threshold off the Proton

W. Bertozzi, S. Gilad, S. Kowalski (spokesperson), S. Sirca,
R. Suleiman (spokesperson and contact person), S. Taylor, Z. Zhou
Massachusetts Institute of Technology

P. A. Souder
Syracuse University

J. P. Chen, K. de Jager, J.-O. Hansen, D. W. Higinbotham, J. LeRose,
N. Liyanage, R. Michaels, S. Nanda, B. Reitz, A. Saha
Thomas Jefferson National Accelerator Facility

L. Kaufman, K. Kumar, K. Paschke
University of Massachusetts

D. Margaziotis
California State University

C. C. Chang
University of Maryland

X. Jiang
Rutgers University

(A Hall A Collaboration Proposal)

November 28, 2001

Abstract

This proposal describes a measurement of the weak pion-nucleon coupling constant to a high level of accuracy using moderate beam time in a theoretically “clean” process. We propose to measure the parity-violating asymmetry in pion photoproduction off the proton, $\vec{\gamma}p \rightarrow n\pi^+$. This asymmetry is expected to be $\sim 2.3 \times 10^{-7}$, and can be measured to statistical uncertainty of $\sim 0.5 \times 10^{-7}$ at Jefferson Lab in Hall A. The systematic errors are expected to be smaller than the statistical errors. The asymmetry is related to the weak isovector pion-nucleon coupling, h_π^1 , with no uncertainty due to nuclear structure. h_π^1 will be determined with uncertainty of 1.0×10^{-7} , 20% of its expected value, 4.6×10^{-7} . At present two completed experiments - photon circular polarization for ^{18}F ($|h_\pi^1| = 0.28_{-0.28}^{+0.89} \times 10^{-7}$) and the anapole moment of ^{133}Cs ($h_\pi^1 = 9.5 \pm 2.1$ [exp.] ± 3.5 [theor.] $\times 10^{-7}$) - have been interpreted to give very different values of h_π^1 . The disagreement in the extraction of h_π^1 from ^{18}F and ^{133}Cs systems could be a reflection of poor understanding of many-body physics. This experiment will be the first attempt to measure the weak pion-nucleon coupling constant in the single nucleon system. A reliable measurement of h_π^1 provides a crucial test of the meson-exchange picture of the weak nucleon-nucleon interaction. Such a test of the meson-exchange picture will shed light on low energy QCD.

1 Introduction

Parity invariance has played a critical role in the evolution of our understanding of the weak interaction. It was the experiment of Wu *et al.* [1] motivated by the suggestion of Lee and Yang [2] that led to re-examination of the symmetry properties of all interactions. In 1958, Feynman and Gell-Mann introduced the $V - A$ interaction for charged currents [3], which, when combined with Weinberg’s introduction of the neutral current a decade later [4], essentially completed our picture of the weak force. Since that time careful experimental work has led to verification of nearly every aspect of the proposed weak interaction structure:

1. in the leptonic sector, $\mu^- \rightarrow e^- \nu_\mu \bar{\nu}_e, \tau^- \rightarrow e^- \nu_\tau \bar{\nu}_e$,
2. in the $\Delta S = 0, 1$ semi-leptonic sector, $n \rightarrow pe^- \bar{\nu}_e, \Lambda \rightarrow pe^- \bar{\nu}_e$,
3. in the $\Delta S = 1$ non-leptonic sector, $\Lambda \rightarrow p\pi^-, K^+ \rightarrow \pi^+\pi^0$.

However, there is one area missing from this itemization: The $\Delta S = 0$ non-leptonic nucleon-nucleon (NN) interactions, $NN \rightarrow NN$. Obviously there is nothing in the identity of the particles involved to reveal the difference between this weak interaction and the ordinary strong $NN \rightarrow NN$ process. In fact the weak NN component is masked by the much larger strong NN force but is detectable by the property of parity violation.

On the experimental side, the first search for parity violation in the NN interaction was carried out by Tanner [5] in 1957, but it was not until 1967 that convincing evidence

was presented for its existence by Lobashov *et al.* [6], who was able to find a $-6 \pm 1 \times 10^{-6}$ signal among the much larger parity-conserving strong background in radiative neutron capture from ^{181}Ta .

Purely hadronic weak interaction between nucleons can be mediated by the exchange of the W^\pm and Z^0 bosons. At momentum transfers typical of the NN interaction, ~ 300 MeV/c, the appropriate degrees of freedom are mesons and nucleons. The range of the W^\pm and Z^0 is $\sim 2 \times 10^{-3}$ fm, much shorter than the distance between nucleons. The hard-core repulsion in the NN interaction keeps the nucleons much farther apart than the range of the weak gauge bosons. The long-range weak force between nucleons is mediated by the exchange of light mesons. As shown in Figure 1, at low energies ($E \leq 300$ MeV), the weak NN interaction is described in terms of an effective meson exchange model in which a meson (π , ρ , or ω) is coupled to a nucleon via the weak interaction at one vertex and the strong interaction at the other. The order of magnitude of the weak meson-nucleon couplings (10^{-7}) can be estimated from a simple scaling argument relating the parity-violating and parity-conserving NN potentials V_{NN}^{PC} and V_{NN}^{PV} , respectively:

$$\frac{V_{NN}^{\text{PV}}}{V_{NN}^{\text{PC}}} \sim G_F m_\pi^2 \sim 10^{-7}, \quad (1)$$

where $G_F = 1.01 \times 10^{-5} M_N^{-2}$ is the weak Fermi coupling constant.

The most comprehensive theoretical treatment to date to describe the weak NN interaction is given in a review by Desplanques, Donoghue, and Holstein (DDH) [7]. They used the non-relativistic quark model, weak SU(6) symmetry, current algebra, and strong SU(3) symmetry to relate known $\Delta S = 1$ hyperon decay amplitudes to the weak meson-nucleon couplings. Because of the hard-core repulsion in the NN interaction, it is customary to include only mesons of mass less than 800 MeV. Parity-violating π^0 and η exchanges would be also CP violating and are therefore suppressed by a factor of about 2×10^{-3} ; as a result neutral pseudoscalar meson (π^0 , η) are excluded from the model. Therefore, only π^\pm , ρ and ω vertices need to be considered and the form of the most general parity-violating effective Hamiltonian is:

$$\begin{aligned} \mathcal{H}_{\text{wk}} &= \frac{h_\pi^1}{\sqrt{2}} \bar{N} (\tau \times \pi)_3 N \\ &+ \bar{N} \left(h_\rho^0 \tau \cdot \rho^\mu + h_\rho^1 \rho_3^\mu + \frac{h_\rho^2}{2\sqrt{6}} (3\tau_3 \rho_3^\mu - \tau \cdot \rho^\mu) \right) \gamma_\mu \gamma_5 N \\ &+ \bar{N} (h_\omega^0 \omega^\mu + h_\omega^1 \tau_3 \omega^\mu) \gamma_\mu \gamma_5 N - h_\rho^{\prime 1} \bar{N} (\tau \times \rho^\mu)_3 \frac{\sigma_{\mu\nu} k^\nu}{2M} \gamma_5 N. \end{aligned} \quad (2)$$

There are in general seven unknown weak couplings. However, calculations indicate that $h_\rho^{\prime 1}$ is quite small [8] and this term is generally omitted, leaving parity-violating observables to be described in terms of just six constants.

Because of uncertainties inherent in the quark model calculations, DDH reported their calculations in terms of broad “reasonable ranges” and “best guess values” of the weak NN interaction coupling constants h_π^1 , h_ρ^0 , h_ρ^1 , h_ρ^2 , h_ω^0 , and h_ω^1 (labeled according

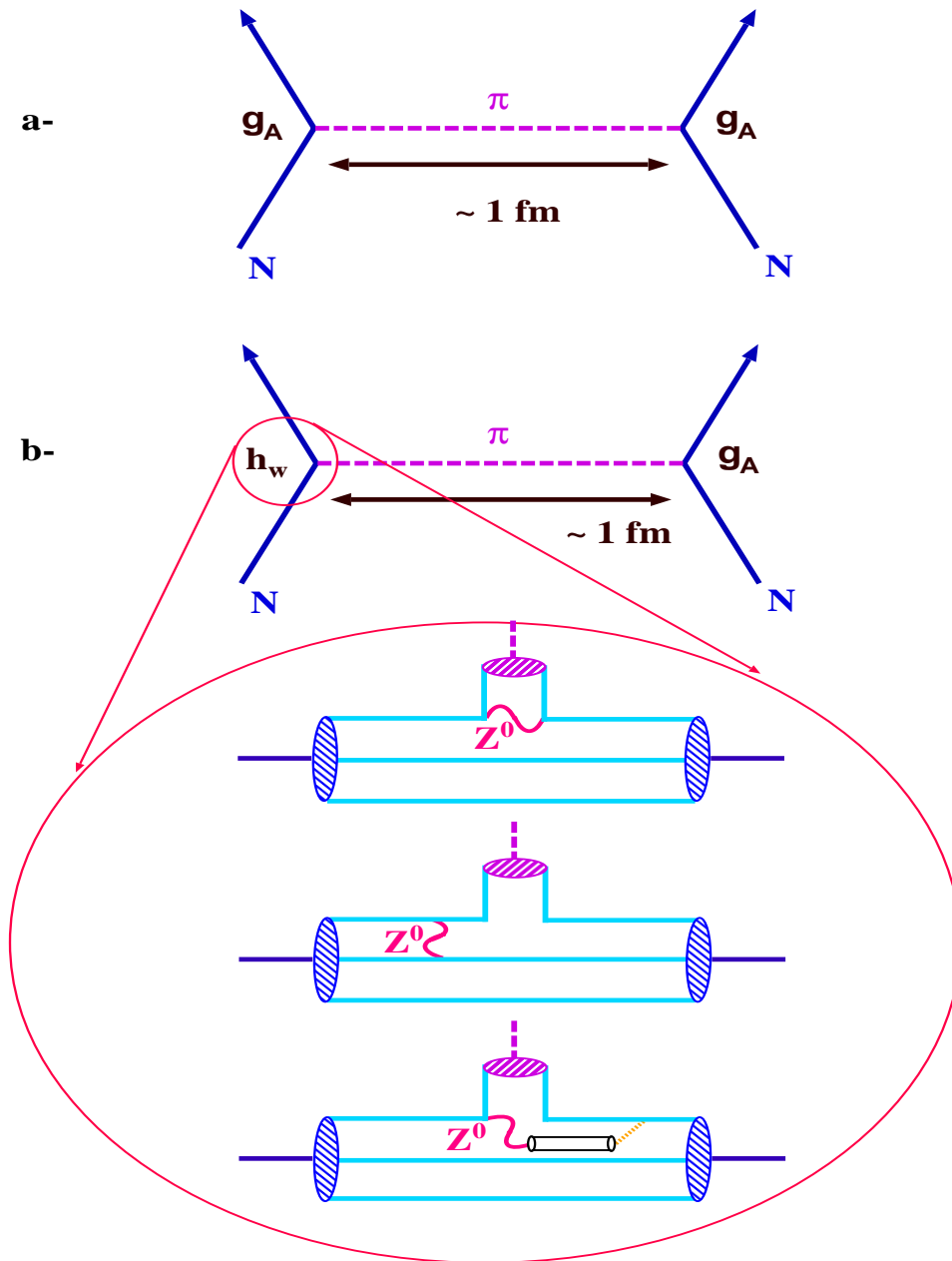


Figure 1: Meson-exchange model of the NN interaction at low energy. (a) Strong meson-exchange, $g_A \sim 1$. (b) Weak meson-exchange, $h_W \sim 10^{-7}$.

to the meson exchange and the isospin exchanged ΔI at the vertex). The determination of these weak meson-nucleon coupling constants from experiment is an essential test of the weak meson-exchange model. The weak pion-exchange potential contributes only to isovector parity-violating processes, and as the pion is relatively light, its contribution is expected to dominate the weak isovector NN interaction at low energy.

1.1 Status of Our Knowledge of the Weak Meson-Nucleon Couplings

An extensive review of the theoretical and experimental work seeking to understand the phenomenon of parity violation within the nucleon-nucleon system is reviewed by Haeblerli and Holstein in Reference [9] and by Desplagues in Reference [10]. A brief summary is given here.

1.1.1 Theoretical Calculations of the Weak Meson-Nucleon Couplings

DDH “best guess values” and “reasonable ranges” for the couplings are given in Table 1. Listed also in the same table, the theoretical predictions of Dubovik and Zenkin (DZ) [11] and of Feldman, Crawford, Dubach, and Holstein (FCDH) [12]. Adelberger and Haxton (AH) [13] extracted from the available data a “best fit” of the weak meson-nucleon couplings.

Coupling	Theoretical (10^{-7})				Experimental (AH) (10^{-7})	
	Range (DDH)	“Best Value” (DDH)	Value (DZ)	Value (FCDH)	Range	“Best Fit”
h_{π}^1	$0 \rightarrow 11.4$	4.6	1.3	2.7	$0 \rightarrow 11$	2.1
h_{ρ}^0	$-31 \rightarrow 11.4$	-11.4	-8.3	-3.8	$-32 \rightarrow 11$	-5.7
h_{ρ}^1	$-0.38 \rightarrow 0$	-0.19	0.39	-0.4	$-0.4 \rightarrow 0.4$	-0.2
h_{ρ}^2	$-11.0 \rightarrow -7.6$	-9.5	-6.7	-6.8	$-10 \rightarrow -6.3$	-6.8
h_{ω}^0	$-10.3 \rightarrow 5.7$	-1.9	-3.9	-4.9	$-12 \rightarrow 2.7$	-6.5
h_{ω}^1	$-1.9 \rightarrow -0.8$	-1.1	-2.2	-2.3	$-3.0 \rightarrow -1.1$	-2.3

Table 1: Theoretical estimates of the sizes of the weak meson-nucleon couplings.

The estimate of h_π^1 from the quark model and weak SU(6) symmetry has been discussed above. Desplanques [14] revised the estimate of the “reasonable range” of h_π^1 to $0 \rightarrow 2.5 \times 10^{-7}$ and the “best value” to 2×10^{-7} . Recently, Henley, Hwang, and Kisslinger [15] used QCD sum rules to obtain h_π^1 . They found that $h_\pi^1 = 3 \times 10^{-7}$, in good agreement with the prediction of DDH. Kaplan and Savage [16] estimated the size of h_π^1 using naive dimensional analysis. Their result of $h_\pi^1 \sim 5 \times 10^{-7}$ is similar to the dimensional estimate of DDH.

1.1.2 Previous Experiments

Measurement of P_γ from ^{18}F and its Interpretation:

The determination of the weak meson-nucleon exchange couplings from experimental measurements in nuclei are discussed in the review by Adelberger and Haxton [13]. There are substantial uncertainties in interpreting most experiments in nuclei because one can not make reliable calculations of the amplitudes of the weak meson-nucleon exchange potential operators. The circular polarization P_γ of the 1.081 MeV transition in ^{18}F is an exception to this unfortunate situation because the matrix elements needed to extract a value for h_π^1 from experiment can be measured experimentally. The circular polarization of a $\Delta I = 1$ parity forbidden gamma transition in ^{18}F has been measured in five different and internally consistent experiments [17]. These measurements gave $|h_\pi^1| = 0.28_{-0.28}^{+0.89} \times 10^{-7}$. This value is a fraction of DDH best guess and is an order of magnitude smaller than the reasonable range.

Measurement of the Anapole Moment of ^{133}Cs and its Interpretation:

The non-zero measurement of the anapole moment of ^{133}Cs [18] has been analyzed by Flambaum and Murray [19] to extract a value for h_π^1 . Their result, $h_\pi^1 = 9.5 \pm 2.1$ [exp.] ± 3.5 [theor.] $\times 10^{-7}$, is a factor of two larger than the DDH value and a factor of seven larger than the upper limit set by the ^{18}F experiments. The situation is summarized in Figure 2. The key question remains the difference between the Fluorine and Cesium results [20]. This highlights the need to determine the weak couplings from experiments in few-nucleon systems and in the single nucleon system whose interpretation is free from uncertainties in nuclear structures.

Experiments in the pp System:

An extensive program of high quality experiments has been carried out to measure the parity-violating longitudinal asymmetry A_z in the scattering of polarized protons off unpolarized protons at 13.6 MeV [$A_z = -0.93 \pm 0.20 \pm 0.05 \times 10^{-7}$] at the University of Bonn [21], and at 45 MeV [$A_z = -1.53 \pm 0.23 \times 10^{-7}$] at SIN in Switzerland (now PSI) [22]. Both results allow the determination of a combination of effective ρ and ω weak

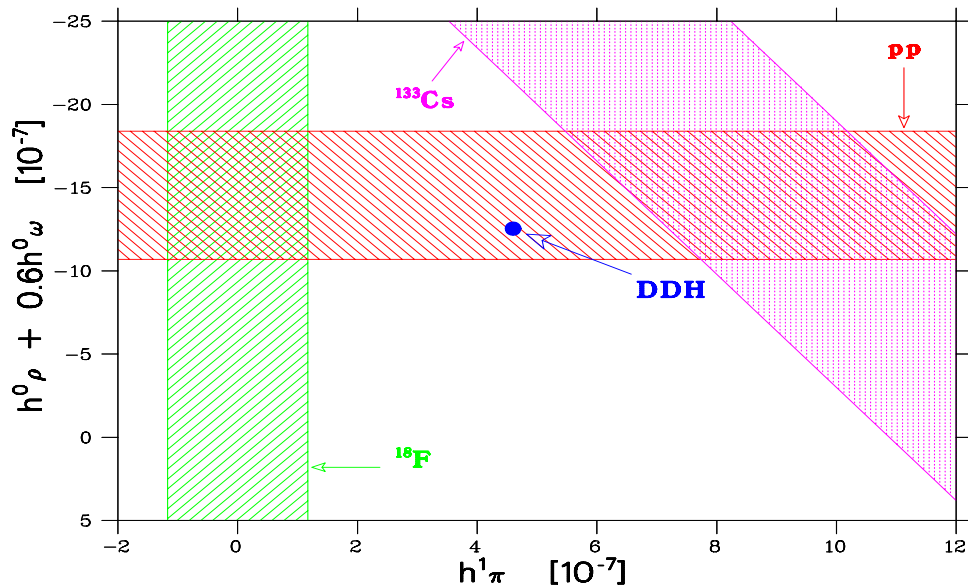


Figure 2: Plot of the constraints on the isoscalar and isovector weak meson-nucleon coupling constants.

meson-nucleon coupling constants:

$$A_z = 0.153 \left(h_\rho^0 + h_\rho^1 + h_\rho^2/\sqrt{6} \right) + 0.113 \left(h_\omega^0 + h_\omega^1 \right) . \quad (3)$$

The TRIUMF 221.3 MeV experiment [23] is sensitive only to the ρ couplings:

$$A_z = -0.0296 \left(h_\rho^0 + h_\rho^1 + h_\rho^2/\sqrt{6} \right) , \quad (4)$$

(note that h_π^1 does not enter due to CP violation). The constraint on the weak meson-nucleon coupling constants from pp experiments is shown in Figure 2.

There exist two further higher energy parity violation experiments. The first one is a $\vec{p}p$ parity violation measurement at 800 MeV with $A_z = 2.4 \pm 1.1 \times 10^{-7}$ at LANL [24]. Its interpretation in terms of the effective ρ and ω weak meson-nucleon coupling constants is more difficult due to the presence of a large inelastic contribution (pion production). The second one is a proton-nucleus parity violation measurement at 5.13 GeV on a water target with $A_z = 26.4 \pm 6.0 \pm 3.6 \times 10^{-7}$ at ANL with the ZGS [25]. This result is much larger than predictions based on meson-exchange calculations. New $\vec{p}p$ parity violation experiments are being planned at TRIUMF possibly at 450 MeV and with COSY at the Forschungszentrum Jülich near 2 GeV as a storage ring experiment [26].

Experiments in the np System:

Measurements have been made in np capture of both the directional asymmetry A_γ and circular polarization of the emitted photons. Both experiments were statistically

limited, and yielded null results. In the first case, Alberi *et al.* [27] reported a value of $A_\gamma = -0.15 \pm 0.47 \times 10^{-7}$, which gives $h_\pi^1 = -1.3 \pm 4.7 \times 10^{-6}$. In the second case, Knyaz'kov *et al.* [28] reported a value of $P_\gamma = 1.8 \pm 1.8 \times 10^{-7}$, which gives $h_\rho^0 + 2h_\rho^2/\sqrt{6} = 8.2 \pm 8.2 \times 10^{-6}$. The inverse reaction, deuteron photodisintegration by circularly polarized photons, has been measured by Earle *et al.* [29], who also report a null result. These experimental limits are less stringent than the reasonable ranges given in Table 1.

While the previous measurements could not reach the required precision, new experiments under way are expected to improve significantly. These include $\vec{n}p \rightarrow d\gamma$ at LANSCE [30]. This experiment will measure the directional asymmetry A_γ of the photons emitted in the capture process which is given by [13]:

$$A_\gamma = -0.107 \left(h_\pi^1 + 0.012h_\rho^1 - 0.035h_\omega^1 \right) . \quad (5)$$

In the experiment, neutrons from the spallation source are moderated by a liquid hydrogen moderator. The source is pulsed, thus allowing measurement of neutron energy through time-of-flight techniques. The cold neutrons are then polarized in the vertical direction by transmission through a polarized ^3He gas. The neutron spin direction can be subsequently reversed by a radio-frequency resonance spin flipper. The neutrons are then captured in a liquid para-hydrogen target. Photons emitted in the capture process are detected in an array of photon detectors surrounding the target. The parity-violating asymmetry causes an up-down asymmetry in the angular distribution of the photons for vertical neutron spin. When the neutron spin is reversed, the up-down photon asymmetry reverses. The parity-violating asymmetry in photon flux,

$$\frac{d\omega}{d\Omega} = \frac{1}{4\pi} (1 + A_\gamma \cos \theta_{s,\gamma}) , \quad (6)$$

is then a measure of h_π^1 . LANSCE experiment will measure A_γ with a statistical error of 0.5×10^{-8} in two calendar years of data taking (9 months of running time). The statistical uncertainty in the extracted value of h_π^1 will be 10% of the DDH estimate while the theoretical uncertainty is estimated to be 10% [31]. The systematic errors are expected to be <1%. This experiment is expected to start commissioning and data taking in 2002. The LANSCE experiment, with its vastly different experimental techniques, should be considered complementary to this proposed experiment.

Another planned experiment at Jefferson Lab [32] will measure the asymmetry in photodisintegration of the deuteron by circularly polarized photons, $\vec{\gamma}d \rightarrow np$. This experiment will measure a combination of the short distance (ρ and ω) weak coupling constants. The pion contribution to this asymmetry vanishes [33] and thus this experiment is not sensitive to h_π^1 .

Experiments in the Single Nucleon System:

This experiment will be the first attempt to measure the weak pion-nucleon coupling constant in the single nucleon system. This measurement is free from nuclear structure uncertainties and is a clean measurement of h_π^1 [34] [35].

2 Pion Photoproduction at Threshold

This experiment will measure h_π^1 by studying pion photoproduction, $\vec{\gamma}p \rightarrow n\pi^+$, with the detection of π^+ . The weak interaction induced parity-violating asymmetries in low energy pion photoproduction were calculated to be of order 10^{-7} by Woloshyn [36] and by Li, Henley, and Hwang [37] in the frame work of meson exchange models. But it is Chen and Ji [34] who first identify the pion photoproduction off proton as an experimentally feasible and theoretically clean process to measure h_π^1 . They found that the photon helicity asymmetry:

$$A_\gamma = \frac{d\sigma(\lambda_\gamma = +1) - d\sigma(\lambda_\gamma = -1)}{d\sigma(\lambda_\gamma = +1) + d\sigma(\lambda_\gamma = -1)} \quad (7)$$

at the first non-vanishing order (NLO) in heavy-baryon chiral perturbation theory (HB χ PT) at threshold is:

$$A_\gamma(\vec{\gamma}p \rightarrow \pi^+n)|_{\text{th}} = \frac{\sqrt{2}f_\pi(\mu_p - \mu_n)}{g_A m_N} h_\pi^1 \sim h_\pi^1/2, \quad (8)$$

where f_π is the pion decay constant ($f_\pi = 93$ MeV) and g_A is the neutron decay constant ($g_A = 1.257$). Figure 3 shows the graphs contributing to the parity-conserving and parity-violating cross sections. In this experiment, there is an extended threshold region in which the effective theory description remains effective and, at the same time, the cross section is appreciable. This region is between 180 and 230 MeV in laboratory photon energy. The higher-order corrections are expected to be $\mathcal{O}(E_\gamma/M_N) \sim 20\%$ and was studied in References [38] and [39]. Additional Chiral corrections to the coupling constant h_π^1 were calculated in Reference [40].

Measuring h_π^1 using pion electroproduction off the proton was also studied by Chen and Ji [41]. The contribution from the Z-boson to the asymmetry and the difficulty in achieving high luminosity due to target boiling make the electroproduction reaction less attractive than the photoproduction one.

The total cross section for $\gamma p \rightarrow n\pi^+$ as a function of photon laboratory energy E_γ is shown in Figure 4. Also shown the $\gamma p \rightarrow p\pi^0$ total cross section. The experimental data are taken from Reference [42]. The solid curve is the leading-order HB χ PT prediction. The leading-order result describes the data (which have considerable variation themselves) within 25% up to $E_\gamma = 230$ MeV. The difference indicates the size of the higher-order corrections expected of HB χ PT and the level of convergence of chiral expansion. Figure 5 shows the differential cross section for $\gamma p \rightarrow n\pi^+$ as a function of the pion CM angle. The small angular variation reflects the dominance of the S-wave contribution. Figure 6 shows the differential cross section as a function of the pion Lab angle.

Figure 7 shows A_γ in the total cross section for $\vec{\gamma}p \rightarrow n\pi^+$ as a function of photon laboratory energy E_γ . The DDH value of $h_\pi^1 = 4.6 \times 10^{-7}$ is assumed. The asymmetry $A_\gamma(\theta^\pi)$ in the differential cross section for $\vec{\gamma}p \rightarrow n\pi^+$ as a function of the pion CM angle is shown in Figure 8 and as a function of the pion Lab angle in Figure 9 ($h_\pi^1 = 4.6 \times 10^{-7}$). Note the strong dominance of the photon polarization asymmetry at forward

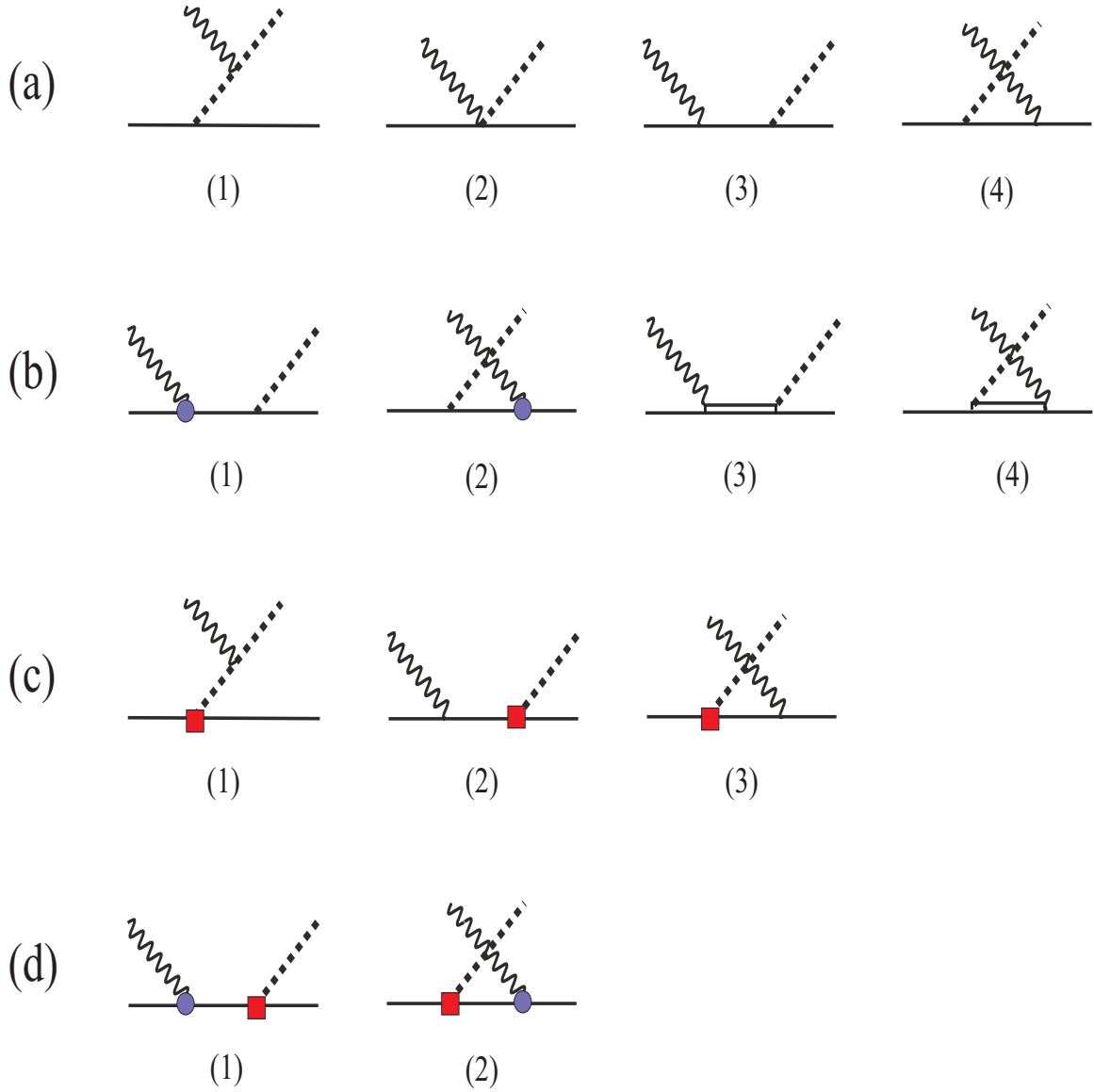


Figure 3: Parity-conserving (PC) leading order (LO) (a) and next-to-leading order (NLO) (b) Feynman diagrams and parity-violating (PV) LO (c) and NLO (d) diagrams for $\vec{\gamma}p \rightarrow n\pi^+$. The wavy lines represent the photons, solid lines the nucleons, dashed lines the pions, and the double lines the Δ resonances. The solid circles denote the NLO PC vertices while the squares denote the PV h_π^1 couplings. The groups (b) and (d) are incomplete but sufficient for the purpose of the asymmetry calculation performed in [34].

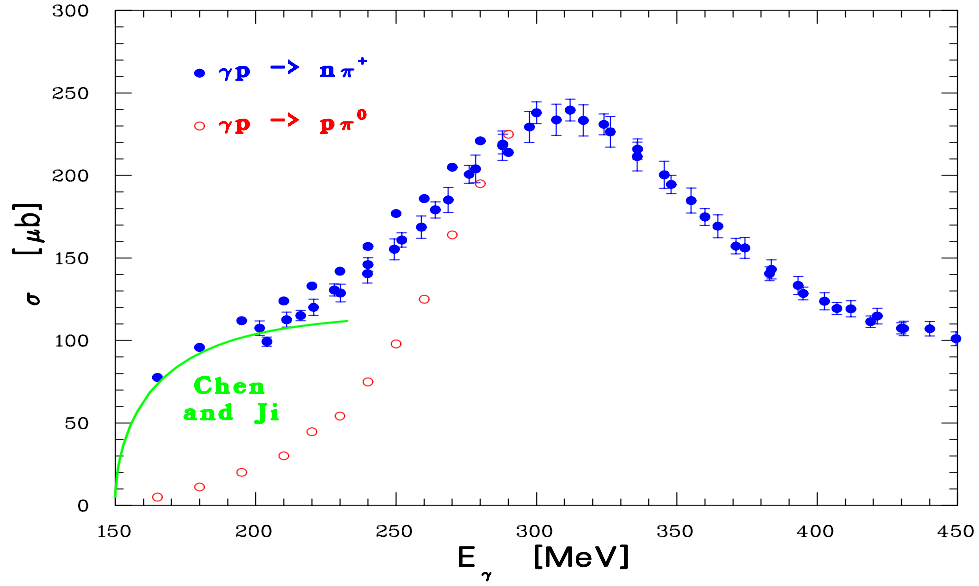


Figure 4: Total cross section for $\gamma p \rightarrow n\pi^+$ as a function of photon laboratory energy E_γ . The experimental data are taken from Reference [42]. The solid curve is the leading-order HB χ PT prediction.

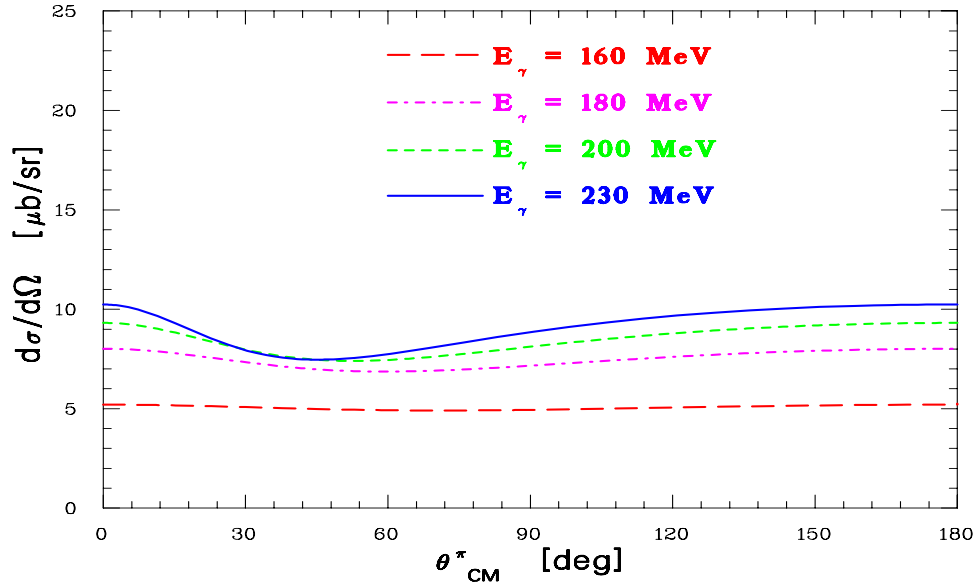


Figure 5: Differential cross section for $\gamma p \rightarrow n\pi^+$ as a function of pion CM angle.

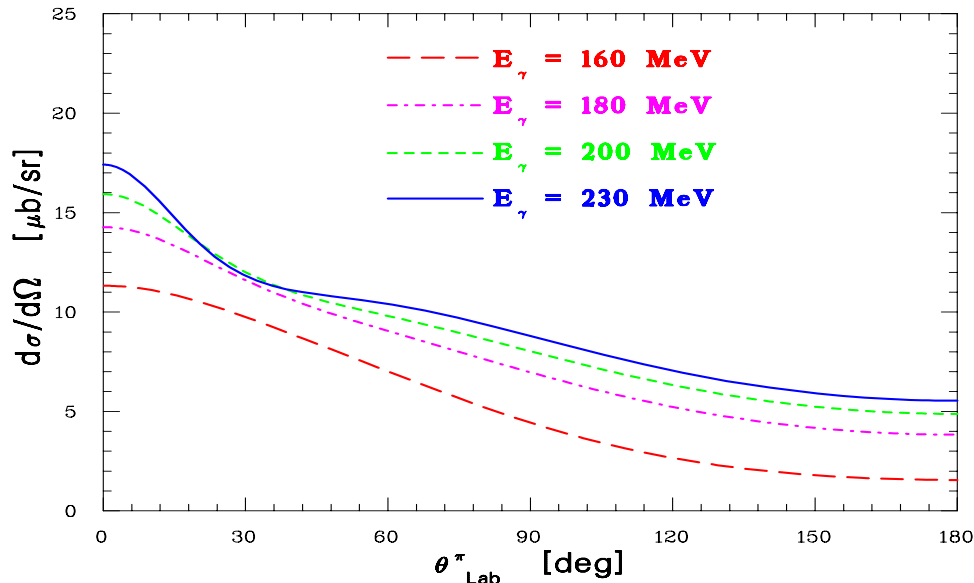


Figure 6: Differential cross section for $\gamma p \rightarrow n\pi^+$ as a function of pion Lab angle.

and backward angles in the threshold region. Only at angles near 90° and $E_\gamma > 200$ MeV does the modification from high partial waves become significant.

2.1 Experimental Considerations

The experiment will take place in Hall A. 400 μA polarized beam with energy of 230 MeV will be used to produce a circularly polarized photons by using 3% *r.l.* Cu radiator. The electron beam will be deflected away through a chicane to the standard Hall A beam dump. The photon beam will be incident on a 80 cm liquid hydrogen target. A toroidal magnet will bend the produced pions to a total absorption plastic scintillator detector. The magnet acceptance will cover the angular range $> 130^\circ$ in theta and 70% of 2π in phi. The expected counting rate is approximately 250 MHz. The detector will be out of direct view of the target and will operate in current mode. Figure 10 shows the proposed experimental setup to study $\vec{\gamma}p \rightarrow n\pi^+$.

The experimental conditions are listed in Table 2. The photon beam polarization is very close to the electron beam polarization. For 200 MeV photon, the polarization is 98% of the electron and for 180 MeV photon, the polarization is 93% (see Figure 11). 1000 hours of beam time are required for 20% statistical accuracy. The total systematic uncertainty is anticipated to be smaller.

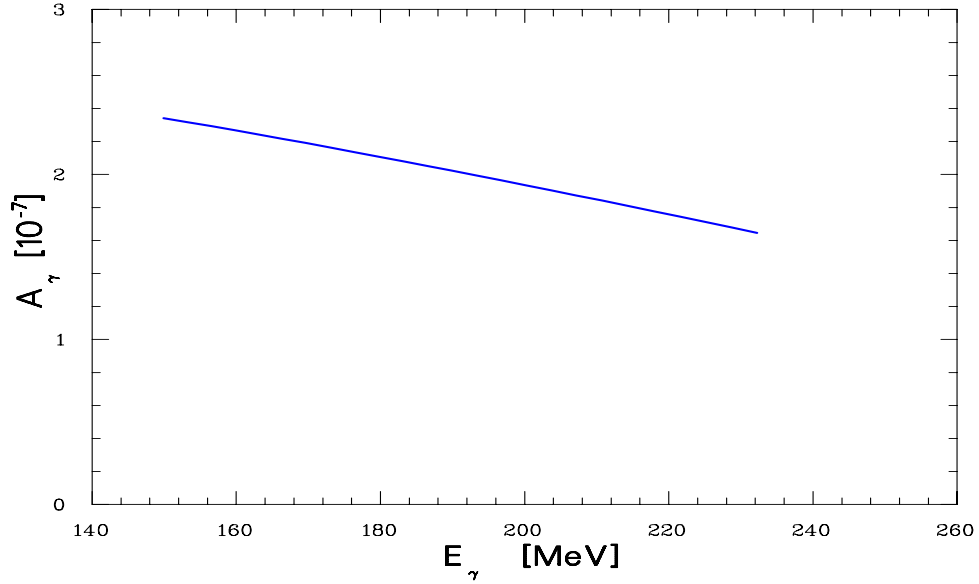


Figure 7: Asymmetry in total cross section for $\vec{\gamma}p \rightarrow n\pi^+$ as a function of photon laboratory energy E_γ ($h_\pi^1 = 4.6 \times 10^{-7}$).

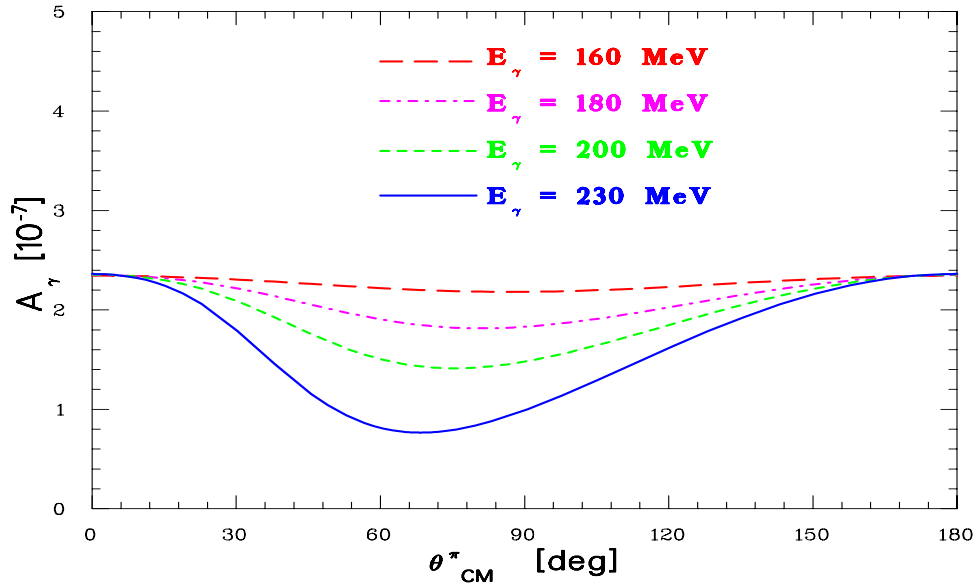


Figure 8: Asymmetry of the differential cross section for $\vec{\gamma}p \rightarrow n\pi^+$ as a function of the pion CM angle ($h_\pi^1 = 4.6 \times 10^{-7}$).

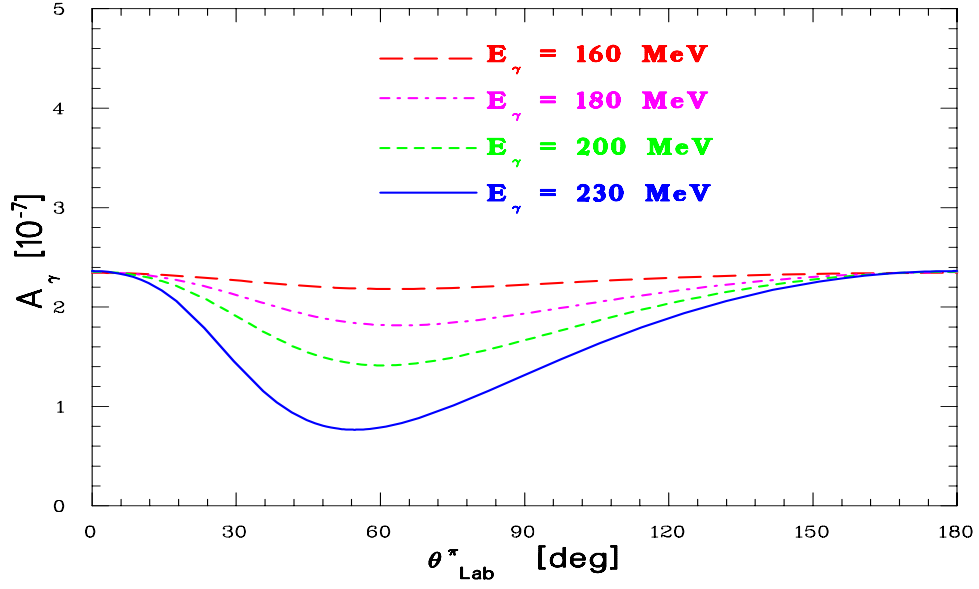


Figure 9: Asymmetry of the differential cross section for $\bar{\gamma}p \rightarrow n\pi^+$ as a function of the pion Lab angle ($h_{\pi}^1 = 4.6 \times 10^{-7}$).

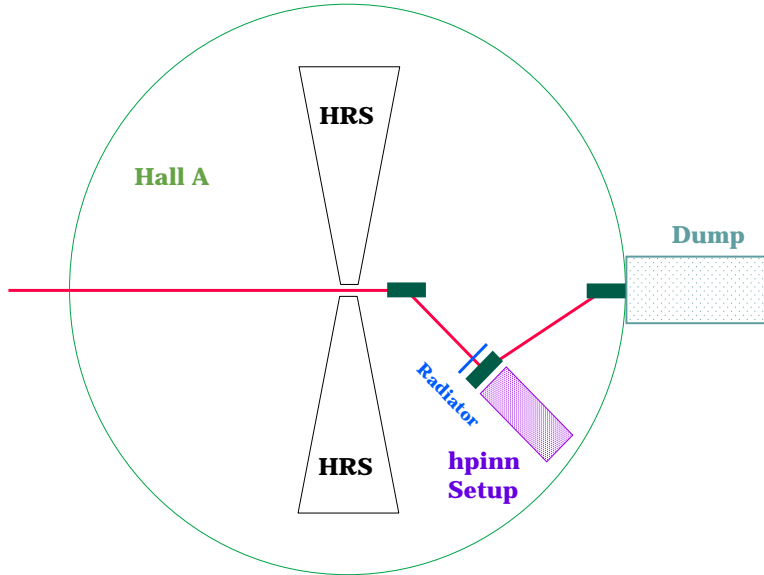


Figure 10: A schematic of the experimental setup in Hall A.

Experimental Hall	Hall A
Beam Energy	230 MeV
Beam Current	400 μA
Beam Polarization	80%
Radiator Thickness	3% <i>r.l.</i> Cu (0.043 cm)
Photon Energy (E_γ)	230-180 MeV
f (N_γ/N_e)	0.006
Photon Polarization	75%
Target	80 cm LH ₂
Luminosity (\mathcal{L})	$0.5 \times 10^{38} \text{ cm}^{-2} \text{ sec}^{-1}$
Theta Angle	$> 130^\circ$
Phi angle	70% of 2π
Solid Angle Acceptance	1.0 sr
Average Cross Section $\frac{d\sigma}{d\Omega}(\gamma p \rightarrow n\pi^+)$	$5 \times 10^{-30} \text{ cm}^2/\text{sr}$
Theoretical Asymmetry (A_γ)	2.2×10^{-7}
Experimental Asymmetry (A)	1.7×10^{-7}
Statistics Needed for 100% Accuracy ($1/A^2$)	3.7×10^{13}
Time Needed for 100% Accuracy	40 hours
Extra Time (Signal Fluctuations)	25%
Total Time (100% Statistical Accuracy)	50 hours
<hr/>	
Total Time (20% Statistical Accuracy)	1000 hours
<hr/>	

Table 2: Experimental conditions for the proposed measurement.

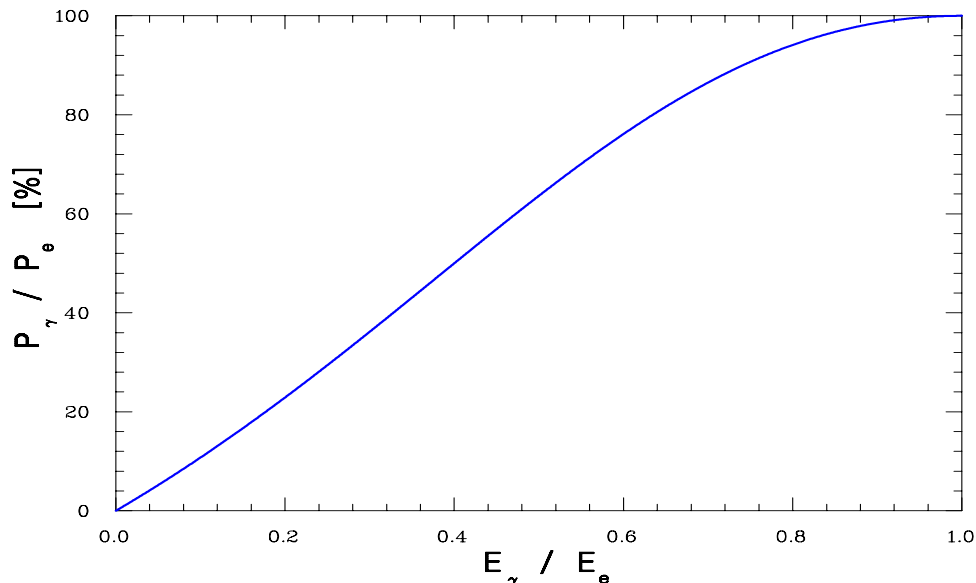


Figure 11: The polarization of the Bremsstrahlung photon as a function of $x = E_\gamma/E_e$ ($P_\gamma/P_e = (4x - x^2)/(4 - 4x + 3x^2)$).

2.1.1 Accelerator and Beam

This experiment requires an electron beam of 400 μA with 80% polarization. The energy of the beam will be 230 MeV. The injector has already produced 550 μA polarized beam with 80% polarization [43]. The accelerator will be able to deliver high quality beam even at this low energy [44]. Note that G0 is already approved to run at 335 MeV [45]. The requirements on the beam quality are the same as the already approved parity experiments at JLab.

It is unlikely that any other experimental hall can run a physics program with such low energy. However, often only two halls are taking data anyway. Sometimes only one hall is taking data. This experiment could run when one or both of the other two halls are open for maintenance. When only one hall is running, the accelerator availability is much greater than 50% which implies that this experiment could be scheduled for less calendar days than usual.

The beam instrumentations such as beam intensity and position will be tested at the proposed current. It is usually the case that the larger the values of the beam signals, the smaller the intrinsic errors. The Mott polarimeter in the injector area and the Møller polarimeter in Hall A will be used to measure the beam polarization.

2.1.2 Hall A

Hall A is the ideal place for this experiment. The experiment will be installed downstream of the standard target pivot in the exit beam pipe area. In this way the experiment will

have minimum impact on Hall A. G0 experiment [45] is occupying the same area in Hall C. HAPPEX [46] already installed and used the DAQ and the beam control devices in Hall A.

2.1.3 Radiator

A 3% Cu radiator will be used to generate the photon beam. The radiator will be located at 3 m upstream of the target. A water cooling system will be used to dissipate the heat deposited in the radiator foil by the electron beam. The electron energy loss in the radiator will be approximately 1 MeV resulting in a heat deposited of 300 W for 400 μ A beam current. The beam will be rastered on the radiator. To keep the beam spot size small, a rotating radiator [47] may be used instead. Local shielding will be placed around the radiator to reduce the background.

Due to Coulomb multiple scattering, the electron beam after traversing the radiator will have an angular distribution with a width given by:

$$\theta_0 = \frac{13.6 \text{ [MeV]}}{\beta pc} \sqrt{0.03} = 9 \text{ mr} \quad (= 0.5^\circ), \quad (9)$$

while the angular distribution of the photon beam has a smaller characteristic angle. Photons with angles greater than 1.0° will be collimated. The angular distribution of the electrons after the radiator and of the photons produced in the radiator are shown in Figure 12 for electron and photon energies greater than 100 MeV.

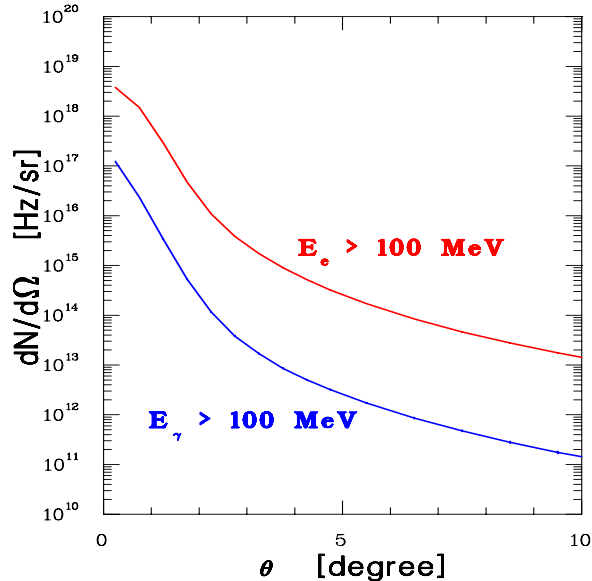


Figure 12: The angular distribution of the electrons after the radiator and of the photons produced in the radiator for electron and photon energies greater than 100 MeV.

The interaction of the electron beam with the radiator was simulated using GEANT [48]. The DINREG [49] code for nuclear fragmentation was implemented within the GEANT package to model medium energy photonuclear and electronuclear reactions. The angular and energy distribution of the photons produced in the radiator are shown in Figure 13.

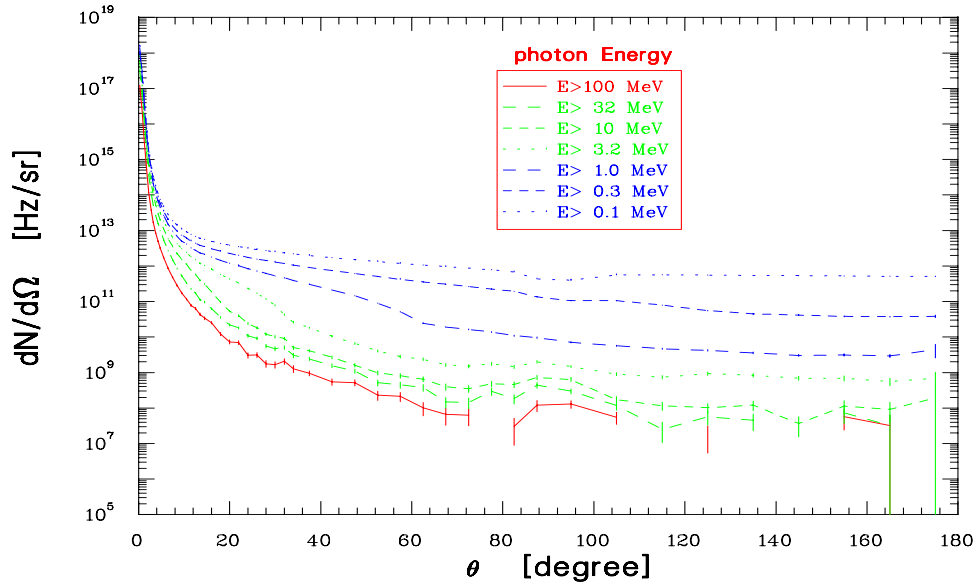


Figure 13: The angular and energy distribution of the photons produced in the radiator.

2.1.4 Sweep Magnet

A dipole magnet will be used to deflect the beam away from the target. For a 45° deflection of 230 MeV electron beam, a 0.6 T.m magnet is needed. The angular and energy distribution of the electrons and positrons after the radiator are shown in Figures 15 and 14. In addition to the sweep magnet after the radiator, there will be a magnet after the normal Hall A pivot to deflect the beam to the radiator at one side of the hall. The third magnet will bend the beam back to the standard Hall A beam dump. All these magnets are available on site.

2.1.5 Target

This experiment will use a 80 cm long liquid hydrogen target. The operating temperature will be 19 K and the operating pressure will be 25 psi giving a target density of 0.072 g/cm^3 .

The target will be approximately 8 cm in diameter. Most of the photon beam will pass through the target (99.7% of photons will pass through a circle with a diameter

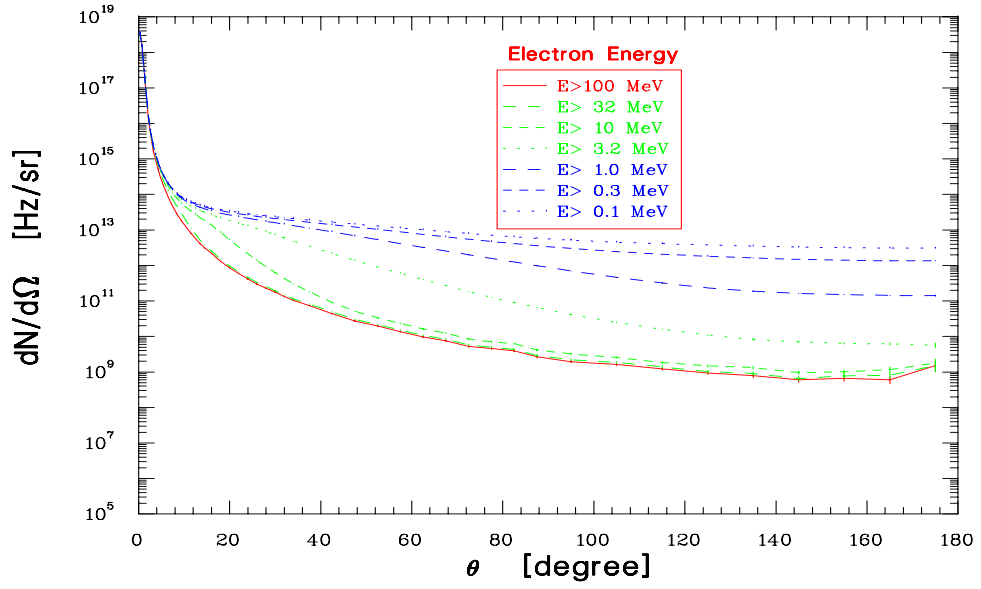


Figure 14: The angular and energy distribution of the electrons after the radiator.

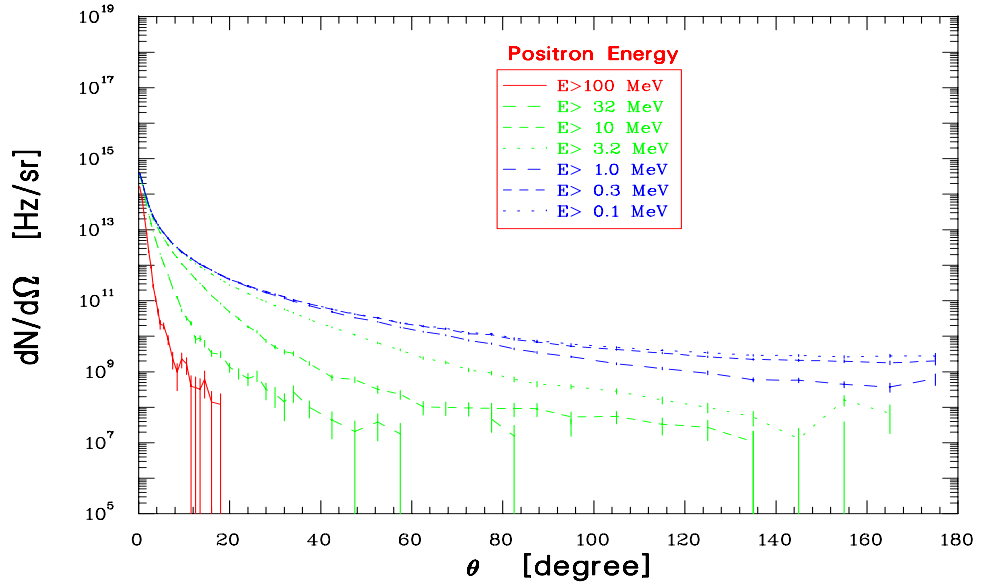


Figure 15: The angular and energy distribution of the positrons after the radiator.

of 5 cm). All surrounding materials, including target walls, flanges and other structures, including the interaction chamber walls, exit pipes and flanges, must be outside the photon beam envelope. The target will require about 100 W of cooling power.

2.1.6 Toroidal Magnet

A toroidal magnet of 3 kG maximum field will be used to bend pions to a detector positioned out of direct view of the target. The magnet will be made of eight resistive Copper coils and would cost about \$200k to build. The magnet parameters are listed in Table 3.

Target Acceptance	80 cm
Momentum Acceptance, Δp	50 – 100 MeV/c
Phi Acceptance, $\Delta\phi$	70% of 2π
Theta Acceptance, $\Delta\theta$	$130^\circ - 180^\circ$
Solid Angle Acceptance, $\Delta\Omega$	1.0 sr

Table 3: Summary of the toroidal magnet parameters.

The magnet is azimuthally symmetric thus the sensitivity to systematic errors associated with beam motion is minimized. There is no magnetized iron, therefore, false asymmetries due to secondary scattering will not be a problem. There is a zero magnetic field at the target position.

2.1.7 π^+ Detector

The detector will be a plastic scintillator of approximately 3 cm in thickness. There will be no problem with spallation in this detector. The detector will act as a total absorber for the pions and will be out of direct view of the target. The detector rate is expected to be 250 MHz and will be readout in integration mode similar to the HAPPEX experiment [46]. The detector consists of eight segments, one per octant, each has a full geometric coverage of the acceptance of the magnet.

The energy detected in the plastic scintillator from pions with momentum of 70 MeV/c is shown in Figure 16. The detector is expected to stand the absorbed radiation dose of 10^6 rad expected over the experiment period. Fluctuations in the energy deposition will result in a non-zero resolution which adds in quadrature to the statistical error according to:

$$\Delta A = \sqrt{\frac{1}{N}(1 + r^2)} , \quad (10)$$

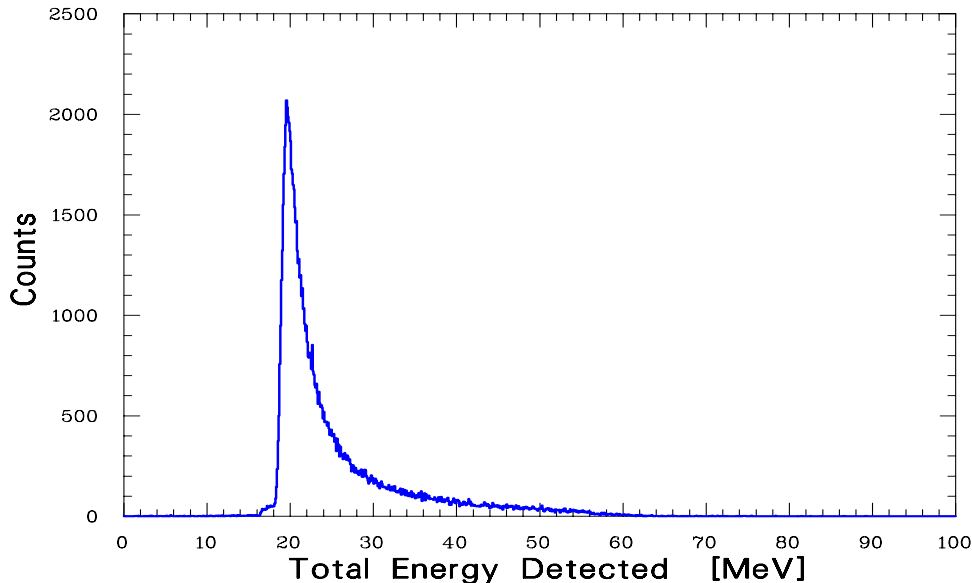


Figure 16: The energy detected in the plastic scintillator from pions with momentum of 70 MeV/c.

where N is the number of detected pions and $r = \Delta E/E$. A bad resolution results in a longer running time to achieve the same accuracy. Statistical fluctuations in the detector is expected to increase the running time by 25%.

A similar detector to the one used to detect pions will be used at forward angle as a luminosity monitor. At forward angle, the photon and e^+e^- rates are huge and no asymmetry is expected. This will serve as a null test for this detector. This luminosity detector is expected to achieve a statistical accuracy of 1×10^{-9} in one hour.

2.1.8 Data Acquisition

We will use the same data acquisition system used during the HAPPEX experiment [46]. The pion signal in the detector will be read in current mode.

2.2 Detector Backgrounds

Table 4 lists the relevant background channels. One source of background is π^0 photo-production which has a cross section comparable to π^+ (see Figure 4). Another source of background will be Compton scattering off the electrons, $\vec{\gamma}e \rightarrow \gamma e$. Most of the background is expected to be low energy forward going particles. The toroidal magnet will be set to detect particles with momenta greater than 50 MeV/c and at a backward angle of $> 130^\circ$ which will help in reducing the charged particles background.

Reaction	Parity-Violating
$\vec{\gamma}p \rightarrow p\pi^0$	“no”
$\vec{\gamma}p \rightarrow \gamma p$	yes
$\vec{\gamma}e \rightarrow \gamma e$	yes
$\vec{\gamma}A \rightarrow e^+e^-$	yes

Table 4: Summary of the background reactions.

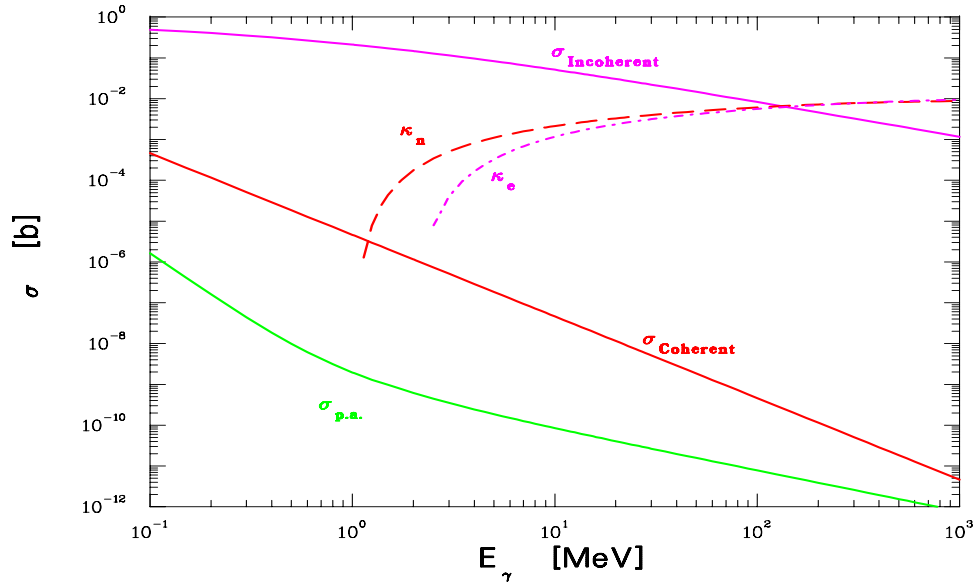


Figure 17: Photon total cross section as a function of energy in LH₂, showing the contributions of different processes [50].

The contributions of different processes to the photon total cross section as a function of energy in LH₂ is shown in Figure 17 [50]. These processes are:

$\sigma_{p.a.}$:	Photon absorption
σ Coherent :	Rayleigh scattering
σ Incoherent :	Compton scattering off an electron
κ_n :	Pair production, nuclear field
κ_e :	Pair production, electron field.

Extensive Monte Carlo simulations is underway to study the experimental setup. Figure 18 shows GEANT geometry of the experimental setup. One major work is to identify the backgrounds in detector (both dilution effect and asymmetry). Especial attention will be given to possible sources of background such as: magnetized iron in dump magnet (including effects from positrons produced in radiator), positrons produced and scattered in target, photon collimator, wide-angle bremsstrahlung and pair production, electron beam dump, and electrons and positrons that miss dump, hit vacuum chamber. Preliminary results are shown below.

The interaction of the photon beam, produced at angle $< 2.0^\circ$ in a 3% Cu radiator by 400 μ A electron beam, in a 80 cm LH₂ target was studied in GEANT. The results are shown in Figures 19-24 where the rate per stradian is plotted as a function of angle.

2.2.1 Photons and π^0 Background

The asymmetry in $\vec{\gamma}p \rightarrow p\pi^0$ ($\pi^0 \rightarrow 2\gamma$) is very small due to CP violation. The A_γ asymmetry in $\vec{\gamma}p \rightarrow \gamma p$ proton Compton scattering was calculated in Reference [51] to be $\ll 10^{-8}(E_\gamma/70 [\text{MeV}])^3$. The A_γ asymmetry in $\vec{\gamma}e \rightarrow \gamma e$ electron Compton scattering was calculated in Reference [52] to be of order:

$$\frac{\alpha m_e^2}{2\pi M_W} \sim 10^{-13} . \quad (11)$$

Therefore, there is no asymmetry in the photons scattered off the target and these photons may only dilute the physics asymmetry.

The backward photons with energies $\lesssim 0.3$ MeV, shown in Figure 19, are the product of Compton scattering off the electrons in the target by the photon beam. The Compton's formula,

$$\frac{1}{\omega'} = \frac{1}{\omega} + \frac{1}{m_e}(1 - \cos \theta) , \quad (12)$$

implies that their energy can not be larger than $m_e/1.7$. Since the detector is out of direct view of the target, another backward scattering off the shielding is required for the photons (by now these photons are x-rays) to reach the detector. The pions would give signals of nearly 20 MeV in the detector. The photons, on the other hand, would only

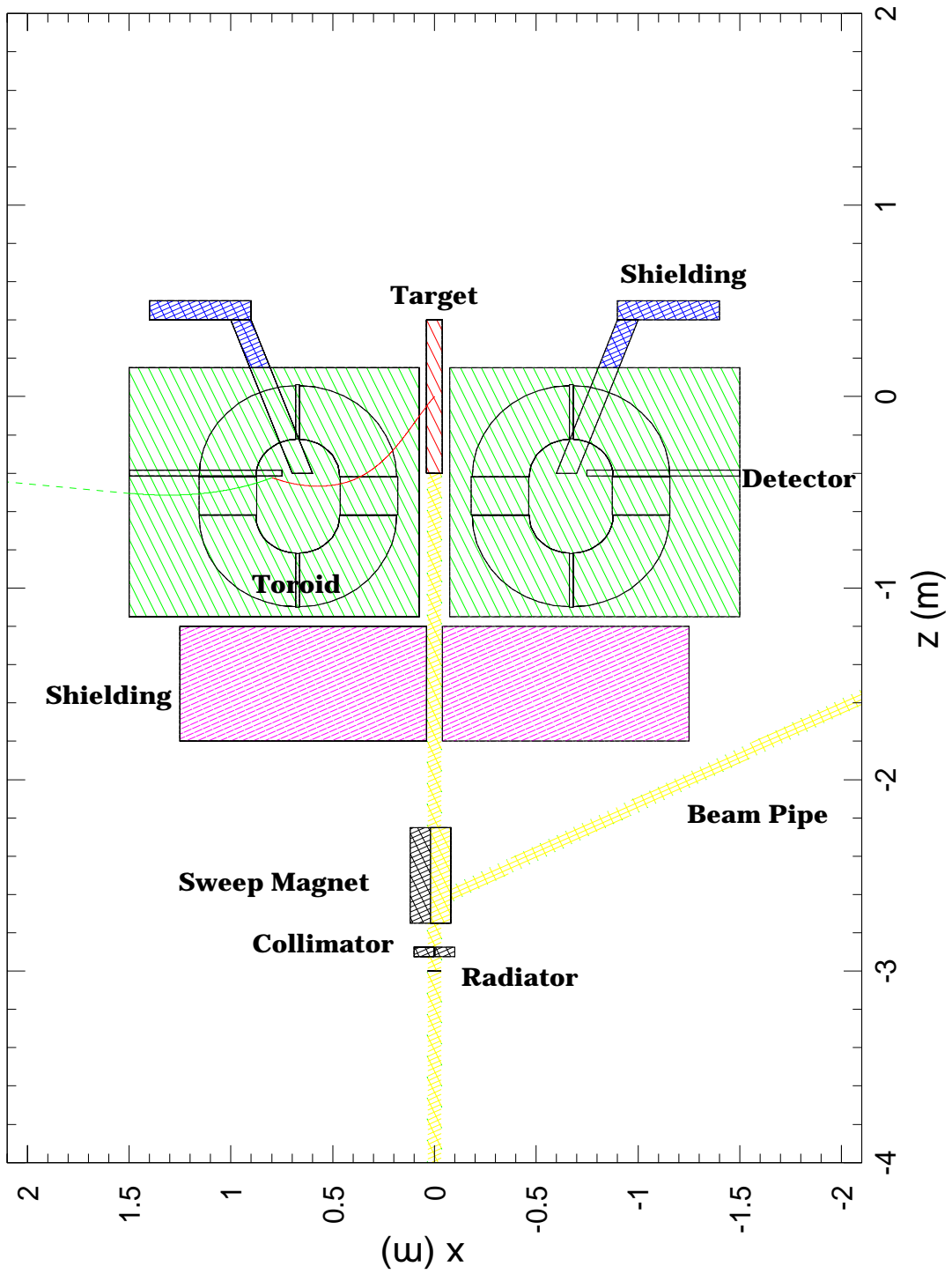


Figure 18: GEANT geometry of the experimental setup.

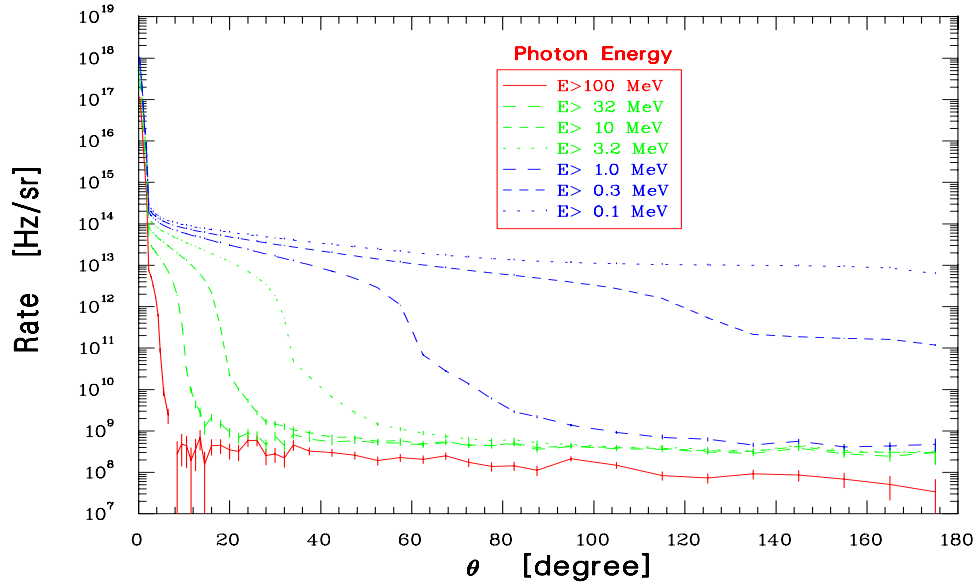


Figure 19: The angular and energy distribution of the photons produced by the photon beam in the target.

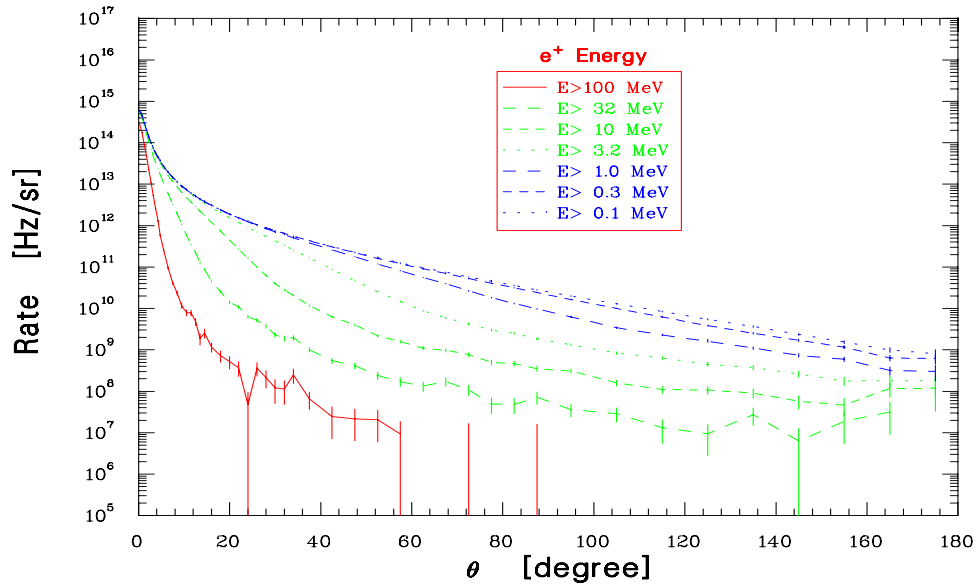


Figure 20: The angular and energy distribution of the e^+ produced by the photon beam in the target.

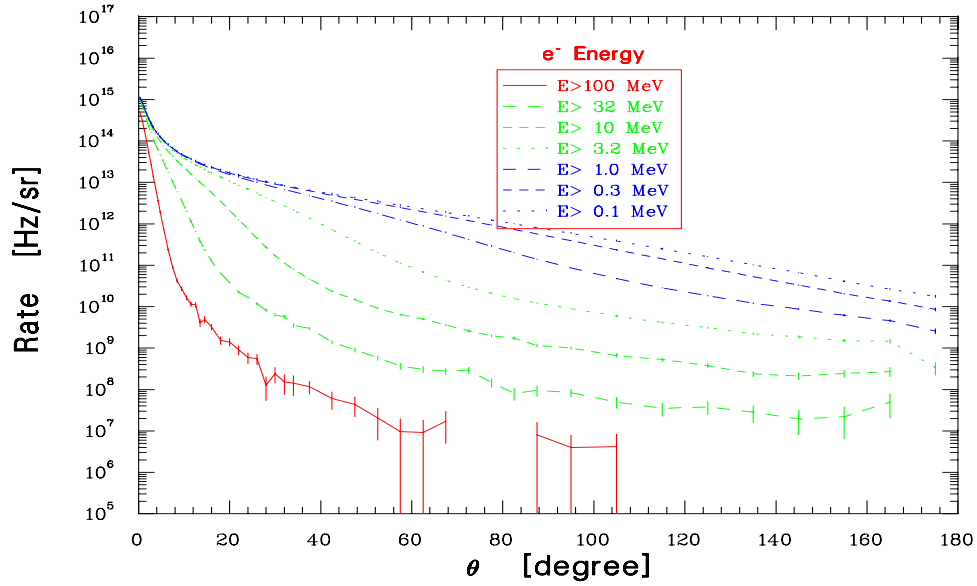


Figure 21: The angular and energy distribution of the e^- produced by the photon beam in the target.

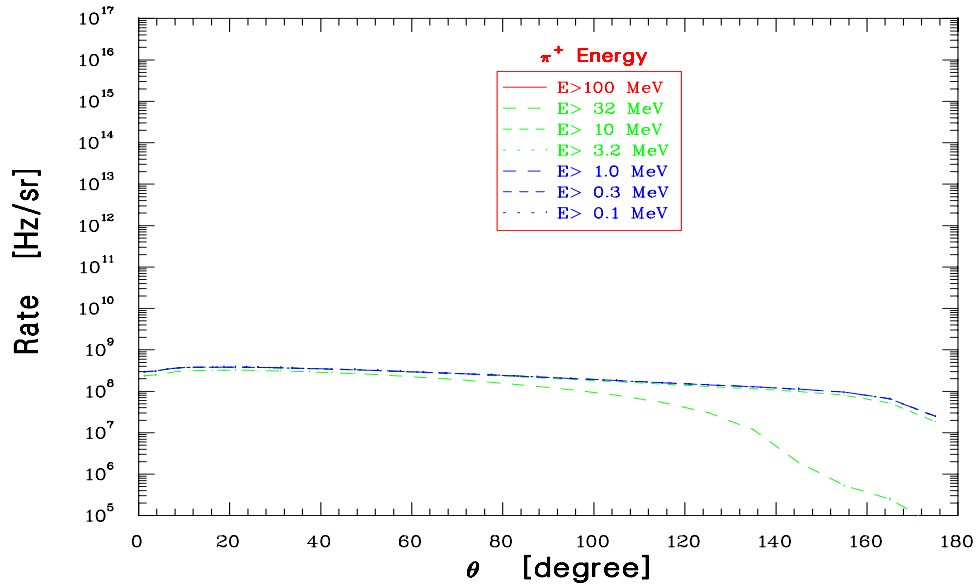


Figure 22: The angular and energy distribution of the π^+ produced by the photon beam in the target.

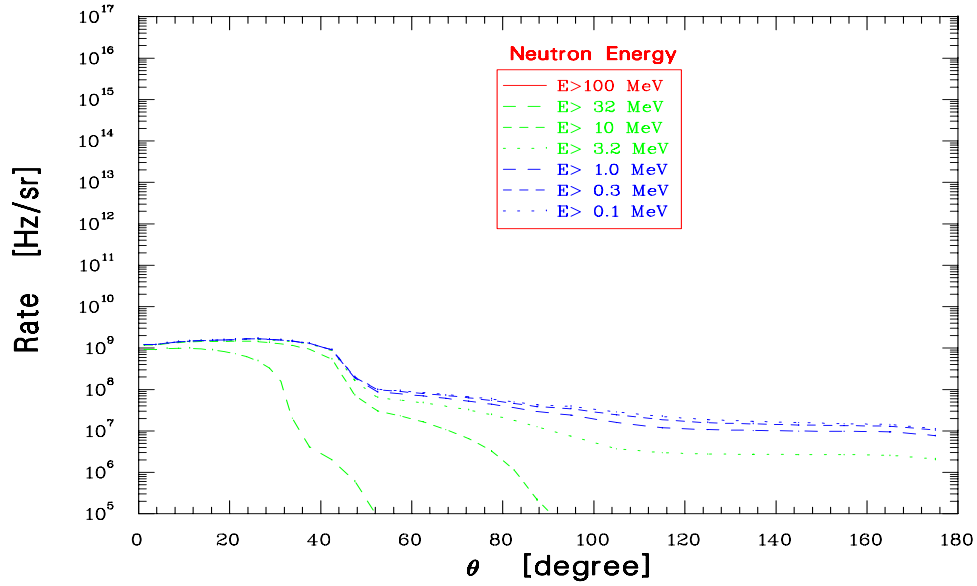


Figure 23: The angular and energy distribution of the neutrons produced by the photon beam in the target.

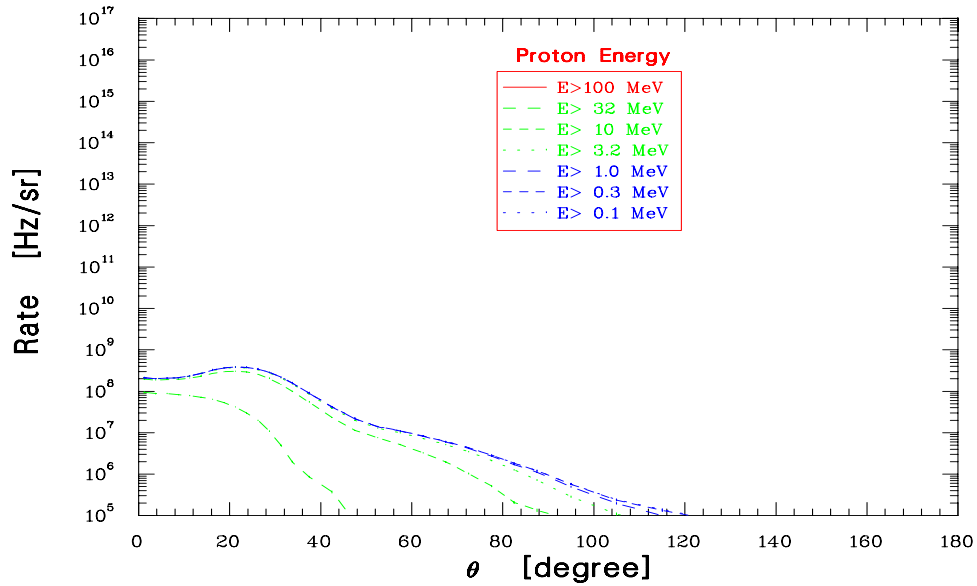


Figure 24: The angular and energy distribution of the protons produced by the photon beam in the target.

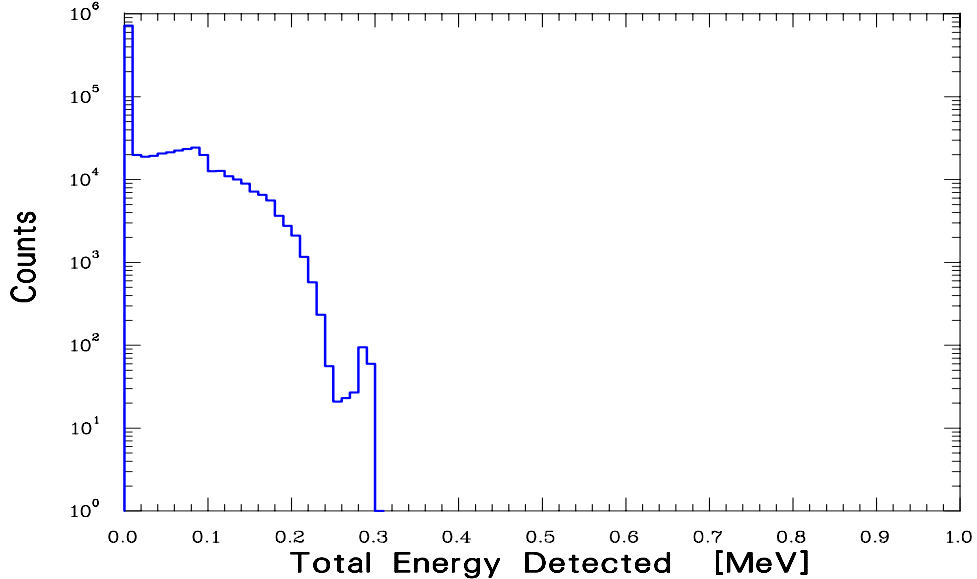


Figure 25: GEANT simulation of the response of the plastic scintillator detector to 0.3 MeV photons.

have a few % probability of interacting in the detector, and even then they would only deposit some fraction of their energy. GEANT simulation of the response of the plastic scintillator detector to 0.3 MeV photons is shown in Figure 25. Therefore, the effect of this background will be a dilution of the asymmetry and will be kept below 10%.

2.2.2 e^+e^- Pair Production Background

The e^+e^- pair production by photons is parity-violating. The A_γ asymmetry in $\vec{\gamma}A \rightarrow e^+e^-$ pair production is estimated to be of the order $\frac{G_F}{\sqrt{2}} \frac{Q^2}{2\pi\alpha} \sim 10^{-4} m_e^2 < 10^{-10}$. The electron and the positron in the pair produced by the photon beam will be polarized at some level with a polarization that will flip with the photon helicity flip. Their degree of polarization depends on their energy and angle [53]. Since there is no magnetized iron in their path, the e^+e^- pairs may only dilute the measured asymmetry. While the electrons will be swept away by the magnet, GEANT simulation shows that the positron rate is $\lesssim 2$ MHz (see Figure 20) which will dilute the measured asymmetry by only 1%. These positrons are produced at backward angles in the pair production process itself and not the result of forward produced positrons scattered backward off protons in the target.

2.2.3 Target Windows Background

The main background from the target windows will be the production of pions. The total thickness of the entrance and exit windows of the target cell will be approximately 0.1

cm of Aluminum. The fraction of π^+ produced in the windows is estimated to be equal to the ratio of protons in the windows compared to protons in the target. Therefore, the windows will contribute on the level of 3%. We assume here that the photon helicity asymmetry is the same as in the case of a free proton (no modification in the nuclear medium).

2.2.4 Neutron Background

The neutron flux from the radiator is shown in Figure 26. More neutrons will come from the photon beam collimator and the sweep magnet area. Part of the neutron background in the detector will come from n-p capture around the detector. Shielding will be placed around the radiator, sweep magnet, and detector to reduce the neutron background. Boron polyethylene is an effective shielding for low energy neutrons. Also, the detector is relatively insensitive to neutrons.

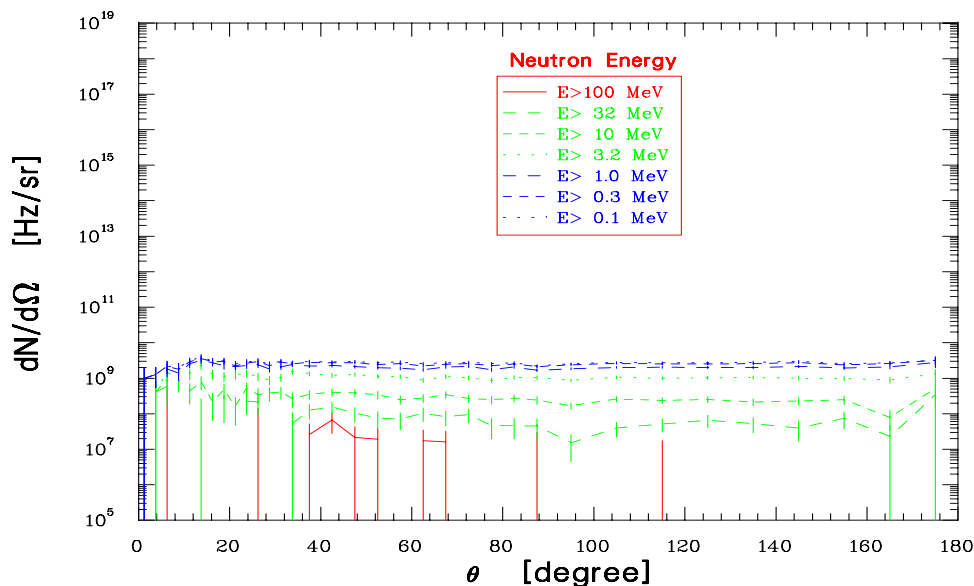


Figure 26: Neutron flux from the radiator. Shielding will be placed around the radiator to reduce the neutron background in the hall.

2.2.5 Pion Decay

The flight path from the target to the detector will be ~ 2 m. For 100 MeV/c pions ($c\tau = 7.8$ m, $\pi^+ \rightarrow \mu^+ \nu_\mu$), 70% will survive to reach the detector. Most of the muons ($c\tau = 659$ m) will make it to the detector so they will not affect the statistics. The muon momentum is 30 MeV/c when the pion decays at rest.

2.2.6 Summary of the Detector Backgrounds

Source of Background	Dilution Effect
x-rays	10 %
e^+	1%

Table 5: Summary of the detector background.

There are only two background contributions in the detector: photons with energy \ll 0.3 MeV and e^+ with energy greater than 50 MeV. Since the parity-violating asymmetries of these backgrounds are much smaller than the measured physics asymmetry, the only effect these backgrounds have is to dilute the physics asymmetry. Table 5 summarizes the detector backgrounds and their dilution effects.

2.3 Systematic Errors

2.3.1 Helicity Correlated Electron Beam and Photon Beam Parameters

Beam Parameter	HAPPEX 98
ΔX	3.3 ± 2.3 nm
ΔY	0.2 ± 2.4 nm
$\Delta\theta_X$	0.05 ± 0.5 nrad
$\Delta\theta_Y$	0.2 ± 0.4 nrad
ΔE	4.4 ± 5.1 eV (@ 3.356 GeV)
ΔI	0.18 ± 0.10 ppm

Table 6: Helicity correlated beam differences achieved during HAPPEX 98 for the electron beam.

The systematic uncertainties due to the electron and photon beams parameters are anticipated to be smaller than the statistical uncertainty. Table 6 lists the helicity correlated beam differences achieved during HAPPEX 98 [54] for the electron beam.

During the 1999 HAPPEX run the corrections due to electron beam parameters were in the worst case $\sim 5 \times 10^{-8}$. The situation will be much improved for future parity experiments at JLab. HAPPEX II [55] will measure an asymmetry to a total systematic error of 3×10^{-8} (only 1×10^{-8} is due to the electron beam false asymmetries). The conditionally approved parity lead radius experiment will measure an asymmetry of $\sim 5 \times 10^{-7}$ to a systematic error $\leq 1 \times 10^{-9}$ [56]. Further, for these two experiments the systematic errors are dominated by the uncertainty in measuring the electron beam polarization. Thus we conclude that the systematic errors due to the injector, electron beam parameters, and DAQ are small. The error in measuring the electron beam polarization for this experiment is only 3%.

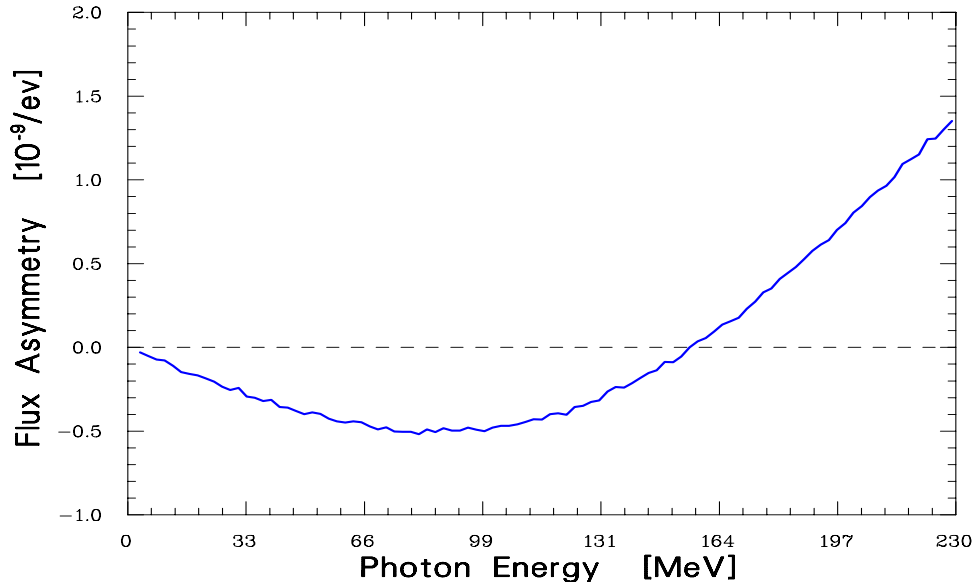


Figure 27: The asymmetry in photon flux from the radiator per 1 eV change in the electron beam energy as a function of the photon energy.

For this experiment, the requirements on the relative precision on the electron beam parameters (energy, angle, and position) are much less stringent than the other parity experiments because the cross section and asymmetry are very insensitive to beam energy and pion production angle (see Figures 6 and 9). At backward angles ($> 130^\circ$), in the region of acceptance, the situation is even much better. Also, the magnet is azimuthally symmetric thus the sensitivity to systematic errors associated with beam motion is minimized.

This high quality electron beam will be used to produce the photon beam *with no amplification* of any of the systematic errors. Careful studies show that the quality of the photon beam will be similar to the electron beam. Figure 27 shows the asymmetry in photon flux from the radiator per 1 eV change in the electron beam energy as a function of the photon energy. We will use photon intensity monitors to measure and control the

photon beam intensity and correct for fluctuations. One possibility is to use Čerenkov detector as a photon intensity monitor. The fluctuations in intensity due to differences in beam position are expected to be very small since only the far tails of the photon beam are collimated.

2.3.2 Parity Violation in Electron Bremsstrahlung

The parity violation in polarized electron bremsstrahlung caused by electroweak interference and weak NN interactions was calculated in Reference [57]. The order of magnitude of the effect is determined by the parameter:

$$\rho = \frac{G_F Q^2}{\sqrt{2} 2\pi\alpha} . \quad (13)$$

In the forward direction and near the maximum of the bremsstrahlung, the parameter ρ is very small ($< 1 \times 10^{-9}$). Thus, the change in the intensity of the photon beam is negligible. The proposed luminosity monitors (in conjunction with the electron beam current monitors) should allow us to regress this out and set experimental limits on its effect.

2.3.3 Linearly and Circularly Polarized Photon Beam

The Bremsstrahlung photon polarization from high energy electrons with arbitrary polarization was studied in Reference [58]. It was found that while Bremsstrahlung is both linearly and circularly polarized (elliptic polarization), the linear polarization is independent of any polarization of the initial electron and circular polarization occurs only for polarized initial electrons. The over all linear polarization of photons produced in a radiator by incoherent Bremsstrahlung vanishes upon integration over all the outgoing Bremsstrahlung cone [59]. The helicity-correlated beam motion could produce a residual linear photon polarization. The contribution of the Σ asymmetry is estimated to be $< 1 \times 10^{-9}$.

2.3.4 Polarized Protons in the Target

Different relative orientations of the two nuclear spins in the diatomic molecule H_2 give rise to the molecular states designated by the prefixes ortho and para. The equilibrium ortho-para composition is temperature dependent. The high temperature concentration of hydrogen, closely approached at room temperature and known as “normal” hydrogen, is 75% ortho-hydrogen (nuclear spins in the same direction) and 25% para-hydrogen (nuclear spins in opposite directions). At 19 K, the equilibrium concentration is 99.82% para and 0.18% ortho.

Due to the presence of magnetic field in the target area, the proton polarization in the target is approximately:

$$P = \frac{\mu_p B}{k T} . \quad (14)$$

For 19 K and taking into account the 0.18% suppression factor, $P \sim 1 \times 10^{-7}/T$. The double polarization asymmetry, $(\sigma_{3/2} - \sigma_{1/2})/(\sigma_{3/2} + \sigma_{1/2})$, for pion photoproduction in the proposed photon energy region is approximately -1 . The toroidal field in the target area will be kept well below 100 G. The systematic error associated with polarized protons in the target is estimated to be $< 1 \times 10^{-9}$.

2.3.5 Summary of the Systematic Errors

Source	Asymmetry	Contribution
Helicity Correlated Beam Fluctuations	1×10^{-8}	6%
Beam Polarization		3%

Table 7: Summary of the systematic errors in this experiment. A total systematic error of less than 10% is expected

The systematic errors specific to this experiment are related mainly to the fact that we are detecting pions in our special detector and to the use of the radiator. Since π^+ is emitted in an S -wave and has spin zero, this prevents any of the photon helicity from leaking directly into the pions. The systematic errors due to detector background are small as discussed in the previous section. The systematic errors in this experiment are summarized in Table 7 where a total systematic error of less than 10% is expected.

3 Parity Violating Photoproduction of π^\pm on the Δ Resonance

Zhu, Maekawa, Holstein, and Ramsey-Musolf [60] analyze the real photon asymmetry A_γ^\pm for the parity violating π^\pm production on the Δ resonance via the reactions $\vec{\gamma} + p \rightarrow \Delta^+ \rightarrow \pi^+ + n$ and $\vec{\gamma} + d \rightarrow \Delta^0 + p \rightarrow \pi^- + p + p$. This asymmetry is non-vanishing due to a PV $\gamma N \Delta$ coupling constant, d_Δ^\pm . An experimental determination of this coupling would be of interest for hadron dynamics, possibly shedding light on the S -wave/ P -wave puzzle in the hyperon non-leptonic decays and the violation of Hara's theorem in weak radiative hyperon decays. The electroproduction case was studied by the same authors in Reference [61].

The expected asymmetry is $A_\gamma^\pm \sim 1.3 \times 10^{-6}$. With two days of running, using the exact setup proposed here to measure h_π^1 but with 330 MeV electron beam, one could achieve a 15% (statistical) determination of A_γ^\pm , which would be more than adequate to address the physics issues considered here.

4 Planned Tests to Demonstrate the Feasibility of This Experiment: Experimental Approach

In addition to a very detailed Monte Carlo simulation of the experimental setup, there will be an extensive experimental studies to demonstrate the feasibility of this experiment. The experimental approach can be divided into three phases:

1. Phase I: This phase consists of parasitic tests to study detector background and demonstrate that the Bremsstrahlung photon beam can be used in a parity experiment. While polarized electron beam is in use in Hall A, the tests would include:
 - Putting the detector at forward angle after the radiator, probably during one of the photodisintegration experiments. The signal will be read using HAPPEX DAQ and the data will be analyzed to check for any asymmetries; none is expected.
 - Putting the detector close to Hall A beam dump. We will try to look for the effect of neutrons and study the amount of shielding required to reduce this background to a negligible level.
 - Studying the backgrounds measured in G0 experiment [45] with especial focus on the background coming from low energy photons.
 - Putting the luminosity monitoring detector at forward angle after Hall A target during HAPPEX II. The target is a 2% radiator and the data will be analyzed to check for any asymmetries; none is expected.
 - Installing the basic setup (magnet, detector, and shielding), when it is ready, close to Hall A target. We will try to test magnet optics, detector response, shielding, and momentum and angular acceptances. We will also try to collect coincidence data between our setup and one of the Hall A spectrometers.
2. Phase II: The experimental setup is ready and installed in Hall A. Using 330 MeV electron beam, we will collect data under the following conditions:
 - Measure the beam parameters derivatives (yield with respect to beam energy, angle, and position).
 - Take data with the toroidal magnet off, with both polarities of the toroidal magnet, and at low current to check the particle id in the detector. A complete detector package installed in one of the octant will be used. This package will include a wire chamber, a Čerenkov detector, and two thin scintillator planes. The goal is to have an experimental verification of the fraction of the detector current that comes from the pions of interest.
 - Take data with empty target to measure the contribution from the pions produced in the target windows.

- Take data with different radiator thicknesses (no radiator, 0.1%, 1.0%, 3.0%, and 10.0% *r.l.*) to study background coming from the radiator. For example, the rate of positrons and neutrons produced in the radiator scales like the square of the thickness, while the rate of electrons that hit the beam pipe after the sweep magnet scales linearly with radiator thickness.
- Test the luminosity monitor detector.

If the above tests were successful then will take production data to measure d_{Δ}^{\pm} . 15 days of beam time are required to carry out the activities of phase II.

3. Phase III: Using 230 MeV electron beam, again carry out the tests done in phase II. If the above tests were successful then will take production data to measure h_{π}^1 . 45 days of beam time are required to carry out the activities of phase III.

5 Milestones and Timeline

The following is a preliminary project milestones and timeline:

1. Demonstrate that a photon beam with the required quality can be achieved and understand the detector background - ongoing task.
2. Finalize the design of the apparatus (with input from both simulation and beam tests) - to be finished in 2002.
3. Start the hardware construction (it is expected to take about 2 years).
4. Commission the experiment and measure d_{Δ}^{\pm} - to be done in 2005.
5. Measure h_{π}^1 - to be done in 2006.

6 Budget and Manpower

The total cost of the experiment is estimated to be \$500k. This is an approved Hall A collaboration experiment. It has the explicit support of K. Kumar, R. Michaels, and P. A. Souder who carried out the HAPPEX experiment and S. Kowalski who has long experience in parity experiments.

7 Radiation Budget

The running conditions for this experiment: 400 μ A of 230 MeV (or 330 MeV) beam on 3% radiator, raise the issue of radiation produced in the hall (both the instantaneous and the integrated radiation. Preliminary calculations done by the Radiation Control Group (RCG) [47] show that this experiment would meet all the requirements including the site

boundary annual design goal limit. The RCG recommended using local shielding around the radiator. Shielding will also be placed on top of the radiator to stop the neutrons from penetrating the roof of the hall.

8 Beam Time Request

We request the following beam time:

- 13 days for planned tests to demonstrate the feasibility of this experiment. Part of the tests will be done parasitic but dedicated running time will be needed to address some of the difficult background issues in this experiment.
- 2 days for production running to measure d_{Δ}^{\pm} .
- 5 days for detector background studies and for photon beam quality check in preparation to measure h_{π}^1 .
- 40 days for production running to measure h_{π}^1 .

The total request of beam time is 60 days (or 1440 hours).

9 Summary

Measurement of parity-violating effects have received much attention in recent years. The $\Delta S = 0$ non-leptonic weak interaction is the last sector of the weak interaction where the main aspects of the electroweak theory are not presently verified. The asymmetry in pion photoproduction will be measured to statistical an accuracy of 20%. This would determine the weak pion-nucleon coupling constant on the same level of accuracy in a reasonable beam time.

Although this experiment and the LANSCE experiment will measure the same coupling constant, these two experiment are completely different: The reaction each used to measure this constant is different, the experimental procedures are different, and the theoretical approaches are also different. These two experiments measuring the same quantity to approximately similar error bar would have a major impact in the nuclear physics. Figure 28 shows the projected error bar compared to other experiments. We ask for the PAC full support to enable this experiment to be scheduled in short period of time.

10 Acknowledgment

We are specially grateful to Jiunn-Wei Chen and Xiangdong Ji from University of Maryland for their most valuable theoretical calculations. We gratefully acknowledge the help from Pavel Degtyarenko for providing GEANT simulations.

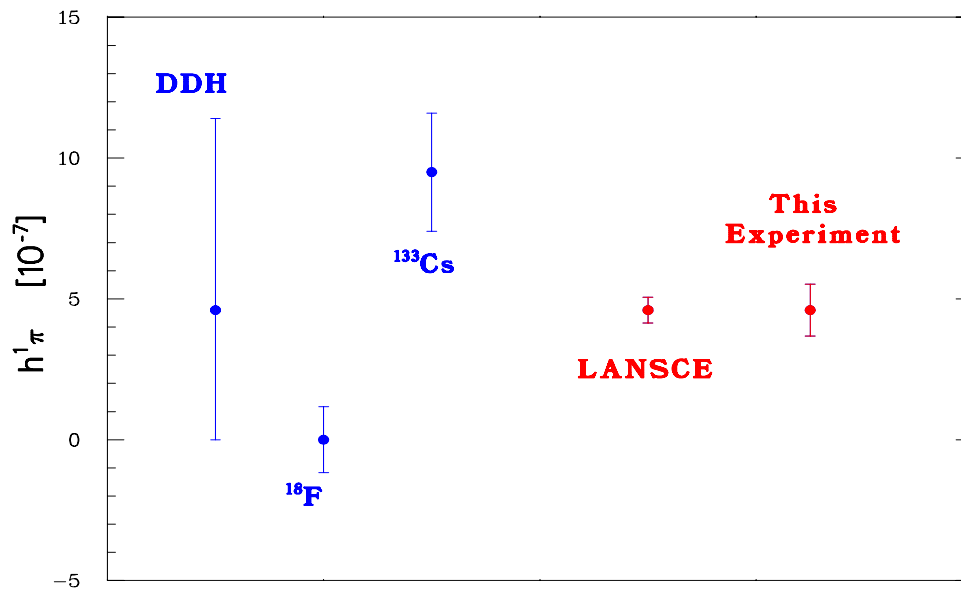


Figure 28: Values of h_π^1 from (left to right) DDH theoretical estimate, ^{18}F experiments, ^{133}Cs experiment, and expected statistical uncertainty from LANSCE experiment (it will achieve this uncertainty in 9 months of data taking). The last value represents the expected statistical uncertainty from this experiment in 1.5 months of data taking.

References

- [1] C. S. Wu *et al.*, Phys. Rev. **105**, 1413 (1957).
- [2] T. D. Lee and C. N. Yang, Phys. Rev. **104**, 254 (1956).
- [3] R. P. Feynman and M. Gell-Mann, Phys. Rev. **109**, 193 (1958).
- [4] S. Weinberg, Phys. Rev. Lett. **19**, 1264 (1967).
- [5] N. Tanner, Phys. Rev. **107**, 1203 (1957).
- [6] V. M. Lobashov *et al.*, JETP Lett. **5**, 59 (1967); Phys. Lett. **B25**, 104 (1967).
- [7] B. Desplanques, J. Donoghue, and B. R. Holstein, Ann. Phys. **124**, 449 (1980).
- [8] B. R. Holstein, Phys. Rev. **D23**, 1618 (1981).
- [9] W. Haeberli and B. R. Holstein, nucl-th/9510062.
- [10] B. Desplanques, Phys. Rep. **297**, 2 (1998).
- [11] V. M. Dubovik and S. V. Zenkin, Ann. Phys. **172**, 100 (1986).
- [12] G. B. Feldman, G. A. Crawford, J. Dubach, and B. R. Holstein, Phys. Rev. **C43**, 863 (1991).
- [13] E. G. Adelberger and W. C. Haxton, Ann. Rev. Nucl. Part. Sci. **35**, 501 (1985).
- [14] B. Desplanques, Phys. Lett. **B512**, 305 (2001).
- [15] E. M. Henley, W.-Y. P. Hwang, and L. S. Kisslinger, Phys. Lett. **B367**, 21 (1996); errata, *ibid.* **B440**, 449 (1998).
- [16] D. B. Kaplan and M. J. Savage, Nucl. Phys. **A556**, 653 (1993).
- [17] S. A. Page *et al.*, Phys. Rev. **C35**, 1119 (1987); M. Bini *et al.*, Phys. Rev. Lett. **55**, 795 (1985).
- [18] C. S. Wood *et al.*, Science **275**, 1759 (1997).
- [19] V. V. Flambaum and D. W. Murray, Phys. Rev. **C56**, 1641 (1997).
- [20] W. C. Haxton and C. E. Wieman, Annu. Rev. Nucl. Part. Sci. **51**, 261 (2001); and private communication.
- [21] P. D. Eversheim *et al.*, Phys. Lett. **B256**, 11 (1991).
- [22] S. Kistryn *et al.*, Phys. Rev. Lett. **58**, 1616 (1987).

- [23] S. A. Page, in “7th Intl. Conf. on Polarization Phenomena in Nuclear Physics”, eds. A. Bourdard and Y. Terrien (Colloque de Physique 51, 1990) C6-253; W. T. H. van Oers, in “Future Directions in Particle and Nuclear Physics at Multi-GeV Hadron Beam Facilities”, ed. D. F. Geesaman (BNL Report BNL-52389, 1993) p.161.
- [24] V. Yuan *et al.*, Phys. Rev. Lett. **57**, 1680 (1986).
- [25] N. Lockyer *et al.*, Phys. Rev. **D30**, 860 (1984).
- [26] W. T. H. van Oers, Invited Paper presented at 16th International Conference on Few-Body Problems in Physics, Taipei, March 6-10, 2000; and private communication.
- [27] J. Alberi *et al.*, Can. J. Phys. **66**, 542 (1988).
- [28] V. A. Knyaz'kov *et al.*, Nucl. Phys. **A417**, 209 (1984).
- [29] E. D. Earle *et al.*, Can J. Phys. **66**, 534 (1988).
- [30] J. D. Bowman (Spokesperson) *et al.*, “Measurement of the Parity-Violating Gamma Asymmetry A_γ in the Capture of Polarized Cold Neutrons by Para-Hydrogen, $\vec{n} + p \rightarrow d + \gamma$ ”, Proposal for DOE, 17 April 1998; W. M. Snow *et al.*, Nucl. Inst. Meth. **A444**, 729 (2000).
- [31] J. D. Bowman and W. M. Snow, private communication.
- [32] JLab LOI 00-002, W. T. H. van Oers and B. Wojtsekhowski, spokespersons (1999).
- [33] I. B. Khriplovich and R. V. Korkin, nucl-th/0010032.
- [34] J. W. Chen and X. Ji, Phys. Rev. Lett. **86**, 4239 (2001); and private communication.
- [35] B. R. Holstein, private communication.
- [36] R. M. Woloshyn, Can. J. Phys. **57**, 809 (1979).
- [37] S. P. Li, E. M. Henley, and W-Y. P. Hwang, Ann. Phys. **143**, 372 (1982).
- [38] J. W. Chen and X. Ji, hep-ph/0101290.
- [39] Shi-Lin Zhu, C. M. Maekawa, B. R. Holstein, and M. J. Ramsey-Musolf, Phys. Rev. **C64**, 35502 (2001).
- [40] Shi-Lin Zhu, S. J. Puglia, B. R. Holstein, and M. J. Ramsey-Musolf, Phys. Rev. **D64**, 33006 (2001).
- [41] J. W. Chen and X. Ji, Phys. Lett. **B501**, 209 (2001).
- [42] F. A. Berends and D. L. Weaver, Nucl. Phys. **B30**, 575 (1971); M. MacCormick *et al.*, Phys. Rev. **C53**, 41 (1996); J. Ahrens *et al.*, Phys. Rev. Lett. **84**, 5950 (2000).

- [43] M. Poelker, CEBAF injector group, private communication; The Science Driving the 12 GeV Upgrade of CEBAF, Draft v1.0, p.131.
- [44] S. Chattopadhyay, CEBAF accelerator group, private communication.
- [45] JLab Proposal E-91-017, D. H. Beck, spokesperson (1991).
- [46] K. Aniol *et al.*, Phys. Rev. Lett. **82**, 1096 (1999).
- [47] P. V. Degtyarenko and R. May, Radiation Control Group, private communication.
- [48] GEANT - Detector Description and Simulation Tool, *CERN Program Library Long Writup W5013*, CERN Geneva, Switzerland (1993).
- [49] P. V. Degtyarenko, M. V. Kossov, and H.-P. Wellisch, Eur. Phys. J. **A8**, 217 (2000); P. V. Degtyarenko and M. V. Kossov, Preprint ITEP 11-92, Moscow (1992).
- [50] National Institute of Standards and Technology, Physical Reference Data, <http://physics.nist.gov/PhysRefData>.
- [51] J. W. Chen, T. D. Cohen, and C. W. Kao, Phys. Rev. **C64**, 055206 (2001).
- [52] E. Bartoš, V. Bytev, and E. Kuraev, hep-ph/0011037.
- [53] J. W. Motz *et al.*, Rev. Mod. Phys. **41**, 581 (1969).
- [54] W. Kahl, Ph.D. thesis, Syracuse University, 2000 (unpublished) and W. Miller, Ph.D. thesis, Princeton University, 2001 (unpublished).
- [55] JLab Proposal E-99-115, K. Kumar and D. Lhuillier, spokespersons (1999).
- [56] JLab Proposal E-00-003, R. Michaels, P. Souder, and G. Urciuoli, spokespersons (2000).
- [57] B. K. Kerimov and M. Y. Safin, Sov. J. Nucl. Phys. **42**, 433 (1985).
- [58] C. Fronsdal and H. Uberall, Nuovo Cimento **8**, 163 (1958); Phys. Rev. **111**, 580 (1958).
- [59] H. Uberall, Phys. Rev. **107**, 223 (1957).
- [60] Shi-Lin Zhu, C. M. Maekawa, B. R. Holstein, and M. J. Ramsey-Musolf, Phys. Rev. Lett. **87**, 201802 (2001); and private communication.
- [61] Shi-Lin Zhu, C. M. Maekawa, G. Sacco, B. R. Holstein, and M. J. Ramsey-Musolf, Phys. Rev. **D65**, in press (2002).

A Appendix I

PAC19 Questions:

a) How can the helicity asymmetry measured by the integrating detector be verified? Considerable attention needs to be paid to the development of:

i) an appropriate current mode detector. The ionization chamber will suffer from spallation noise due to reactions in entrance windows, which will affect the accuracy of the measurement.

The proposed toroidal magnet and scintillation detector combination deals well with the PAC concern about spallation background in the previously proposed ionization chamber.

ii) a null test for this detector.

Addressed by the use of a forward detector in Phase II. It is not an ideal null test, since it is measuring different particles than the pions, however it provides a null test of the electronics, target, and photon beam monitoring.

iii) an experimental verification of the fraction of the detector current that comes from the pions of interest.

Addressed in Phase II of the run plan. A complete detector package will be installed in one octant. This package will include a wire chamber, a Čerenkov detector, and two thin scintillator planes. A sensible program of background measurements (varying radiator thickness, empty target, etc.) is outlined in Phase II.

iv) a calibration measurement of the parity violating asymmetry is there a known parity violating asymmetry that can provide such a test?

The measurement of the much larger expected asymmetry in the Delta photo-production experiment will partly act as a calibration measurement. The Delta asymmetry measurement is an attractive extra feature, both as a shakedown run, and for the physics impact in its own right.

b) How big are helicity correlated backgrounds from particles interacting with iron in the sweep magnet that deflect electrons to the dump? Many low energy electrons and all of the positrons produced in the radiator will not make it to the dump.

The PAC's concerns about helicity-correlated backgrounds from the sweeping magnets are dealt with by reducing the thickness of the radiator. This also allows for dumping the beam in the standard Hall A dump instead of a local beam dump as previously proposed. A full program is outlined in phase II to deal with neutron, electron, and positron backgrounds after the radiator. These backgrounds have different dependence on the radiator thickness. Shielding in the sweep magnet area will also help in reducing these backgrounds.